



# Continental-scale erosion and transport laws: A new approach to quantitatively investigate macroscale landscapes and associated sediment fluxes over the geological past

**Martine Simoes**

*Géosciences Rennes, UMR 6118, Université Rennes 1, CNRS, Campus de Beaulieu, F-35042 Rennes, France*

*Now at Institut de Physique du Globe de Paris, UMR 7154, Université Paris 7, CNRS, Equipe de Tectonique, Bureau 213, 1 rue Jussieu, F-75238 Paris, France (simoes@ipgp.fr)*

**Jean Braun**

*Géosciences Rennes, UMR 6118, Université Rennes 1, CNRS, Campus de Beaulieu, F-35042 Rennes, France*

*Now at Laboratoire de Géologie des Chaînes Alpines, UMR 5025, Université Joseph Fourier, CNRS, BP 53, F-38041 Grenoble, France*

**Stéphane Bonnet**

*Géosciences Rennes, UMR 6118, Université Rennes 1, CNRS, Campus de Beaulieu, F-35042 Rennes, France*

[1] Although critical to a variety of issues in Earth Sciences, paleotopography remains poorly constrained over the geological past. Indeed, sediments preserve a record of the history of the Earth surface, but deconvolving these archives remains a challenge in the absence of a proper quantification of surface processes at the large spatial and temporal resolution imposed by these data. To solve for this, we propose a set of simple bedrock erosion and sediment transport laws that apply over large spatial (~100 km) and temporal (~1–10 Ma) scales. These laws are tested in light of physical experiments of landscape evolution under different tectonic and climatic forcings and are calibrated using present-day large-scale Earth topography and sediment fluxes in rivers. We subsequently implement these processes into a numerical code, TopoSed, that is able to predict the evolution of macroscale topography, sediment fluxes, paleogeographies, and bedrock exhumation given a tectonic and climatic input scenario. The results of such simulations can be directly compared to sedimentary or thermochronological data to test the plausibility of the input tectonics and predicted topography. A series of tests on the sensitivity of such predictions to the uncertainties on input parameters shows that it should be possible from sedimentary data to invert for paleouplift rates and also for paleotopographies during periods covering major tectonic or climatic events. Although this code is meant to be refined in the future as we improve our understanding of surface processes at these macroscales, TopoSed provides a powerful tool to put constraints on past geodynamic processes, such as dynamic topography, by extracting quantitative information on the evolution of the Earth surface from sedimentary data.

**Components:** 13,700 words, 14 figures, 3 tables.

**Keywords:** surface processes; topography; sedimentology; thermochronology; stratigraphy; geodynamics.

**Index Terms:** 1824 Hydrology: Geomorphology: general (1625); 8169 Tectonophysics: Sedimentary basin processes (0905); 8110 Tectonophysics: Continental tectonics: general (0905).

**Received** 9 March 2010; **Revised** 8 June 2010; **Accepted** 17 June 2010; **Published** 2 September 2010.

Simoes, M., J. Braun, and S. Bonnet (2010), Continental-scale erosion and transport laws: A new approach to quantitatively investigate macroscale landscapes and associated sediment fluxes over the geological past, *Geochem. Geophys. Geosyst.*, **11**, Q09001, doi:10.1029/2010GC003121.

## 1. Introduction

[2] Paleotopography is key to understand the Earth's system. For example, the topography and large-scale morphology of the Earth affects climate by perturbing atmospheric circulation [e.g., Fluteau *et al.*, 1999; Sepulchre *et al.*, 2006], by focusing erosion and silicate weathering [e.g., Gaillardet *et al.*, 1999], by stabilizing petrogenic carbon [Galy *et al.*, 2008] or by burying present-day organic carbon [Galy *et al.*, 2007]. On the other hand, the topographic evolution of the continents is the result of rock uplift over geological periods and, as such, is the product of forces acting within the Earth's interior. It therefore appears key to assess and discriminate past geodynamic processes [e.g., Conrad and Gurnis, 2003]. Although critical to a variety of issues in Earth sciences, topography has remained poorly quantified over the long-term mostly because it reflects the interplay between deep and surface processes [e.g., Avouac and Burov, 1996; Bonnet and Crave, 2003; Whipple and Meade, 2006]. Usual attempts come from paleoaltimetry, but these studies are usually local and only focus on most recent tectonic events [e.g., Rowley and Garzzone, 2007]. There are also simple 1D investigations [Pazzaglia and Brandon, 1996] or paleogeographic maps where topography is reconstructed based on qualitative assumptions between present-day topography and tectonic context (e.g., C. R. Scotese, PALEOMAP Project, 2001, available at <http://www.scotese.com>). A rigorous methodology to quantify paleotopographies and paleouplifts over geological times is however lacking.

[3] Sediments in basins have preserved a record of the evolution of the Earth surface. However, one of the major challenges in deconvolving the sedimentary record and in retrieving this evolution is to define appropriate surface processes laws that describe how the landscape and sediment fluxes evolve over time as a response to tectonic and climatic forcings (Figure 1) [e.g., Allen, 2008]. Following Kooi and Beaumont [1996], we consider

three scales at which surface processes can be analyzed. At a microscale, elementary physical geomorphic processes have been extensively investigated following a mechanistic approach [e.g., Sklar and Dietrich, 2004]. Several attempts to upscale these processes to laws of fluvial incision or hillslope processes (mesoscale) have followed [e.g., Davy and Crave, 2000; Howard *et al.*, 1994; Lavé, 2005; Sklar and Dietrich, 2006; Whipple and Tucker, 1999], and these laws are now extensively used in regular models of landscape evolution [e.g., Braun, 2006; Dietrich *et al.*, 2003; Tucker and Slingerland, 1997; Tucker and Bras, 1998; Tucker and Hancock, 2010] or of orogenic response to tectonic or climatic forcings [e.g., Godard *et al.*, 2006; Whipple and Meade, 2004, 2006]. At the even much larger scale imposed by the spatial and temporal resolution of most sedimentary data (Figure 1), that is, over large continental surfaces (~100s to 1000s km) and over long geological periods (~1 to 100s of Ma), the refinement of such landscape evolution models is computationally and unnecessarily too demanding, in particular because the details of past landscapes are usually unknown at the scale of channels and hillslopes (Figure 2). In fact, sediment production and transport have been poorly investigated at this macroscale.

[4] At large spatial scales, attempts to provide simple surface processes laws come from possible correlations between present-day sediment fluxes measured at the mouth of major rivers worldwide, and morphometric and climatic parameters of their drainage basins [e.g., Ahnert, 1970; Hay, 1998; Ludwig and Probst, 1998; Milliman and Syvitski, 1992; Pinet and Souriau, 1988; Summerfield and Hulton, 1994; Syvitski and Milliman, 2007]. Most authors have subsequently proposed a macroscale erosion law in which erosion is essentially related to mean elevation or basin relief, and eventually to climate. However, no clear systematic relation has come out of these analyses [Hay, 1998; Ludwig and Probst, 1998]. This is in part because the significance of a mean value for some of the

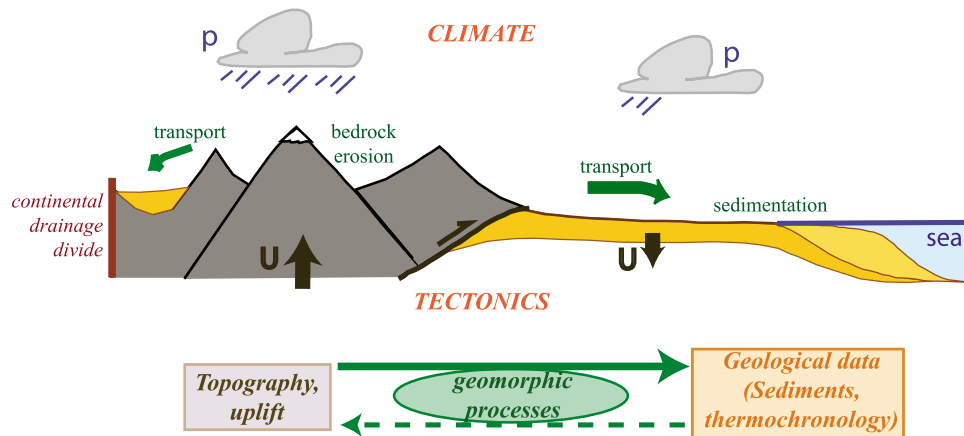


**Figure 1.** Schematic representation of the evolution of continental surfaces under climatic and tectonic forcings. This evolution can be complex when considered over large spatial scales, with continental sediment storage in alluvial plains or internal basins [Allen, 2008]. However, it can be properly deciphered from sedimentary records (paleogeographies, sediment fluxes, etc.) provided appropriate laws for geomorphic processes (i.e., bedrock erosion and sediment transport) that act as transfer functions between this evolution and the actual data.

parameters (e.g., temperature, precipitation) over very extensive areas can be questioned, or else because present-day measured detrital fluxes may not be relevant over longer time periods [Kirchner

*et al.*, 2001] as they may not capture discrete extreme flood events during which a large volume of sediments is transported to the ocean [Dadson *et al.*, 2004; Meade and Parker, 1985]. Also, these

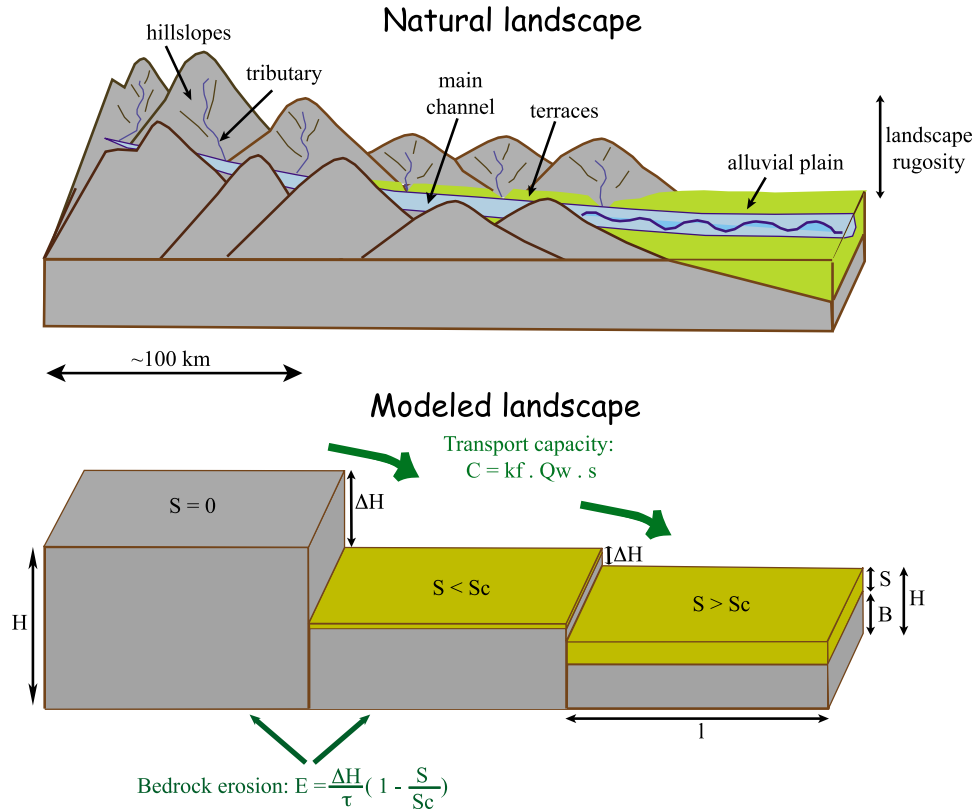


**Figure 2.** Schematic view of how we propose to upscale the different elements of natural landscapes. Our approach does not capture the details of the landscape (hillslopes, channels, etc.) but rather considers a simple mass budget of bedrock and sediment at a regional scale (~100 km unit spatial scale). We propose that microscale and mesoscale geomorphic processes can be upscaled to simple relationships, as in equations (2) to (9).

sediment fluxes integrate several complex processes (sediment production by a wide range of erosion mechanisms/transport/storage in alluvial plains, etc.) that cannot be solved separately from such analyses [Aalto *et al.*, 2006; Allen, 2008]. Over longer timescales of 100 years to 1 Myr, denudation rates have been derived from cosmogenic nuclide analyses [e.g., Binnie *et al.*, 2007; Ouimet *et al.*, 2009; Riebe *et al.*, 2001, 2004; Schaller *et al.*, 2001; von Blanckenburg *et al.*, 2004; von Blanckenburg, 2005], but the resulting fluxes still integrate different geomorphic processes that encompass a large range of production and transport mechanisms. Integration of mesoscale fluvial and hillslope erosion laws into numerical models indicate that the macroscale behavior of landscapes is complex [Kooi and Beaumont, 1996] and scale-dependent [Davy and Crave, 2000]. These results do not provide however simple guidelines to quantitatively analyze the evolution of continental surfaces. Recently, physical experiments of macroscale topography and denudation evolution with different lithologies and under different uplift and precipitation rates, in which the transient and equilibrium response of the system could be monitored, have been developed in an attempt to better understand landscape response to a variety of forcings [Babault *et al.*, 2005; Bonnet and Crave, 2003, 2006; Lague *et al.*, 2003]. Because steady state denudation and sediment fluxes solely depend on uplift rate in these experiments, they suggest that it is possible, in theory, to discriminate in the sedimentary record between changes in tectonic or climatic forcings [Bonnet and Crave, 2003].

[5] The purpose of our study is to provide a set of simple plausible transfer functions that can be used for the inversion of sedimentary data into paleotopographies and paleouplift rates. The laws proposed here can be regarded as an attempt at upscaling different elementary processes and fluvial incision laws over continental scales (~100s to 1000s km) and/or over geological times (~1 to 100s Ma) (Figure 2). Because our primary objective is to provide a tool for retrieving realistic quantitative constraints on past macroscale landscapes from geological data, we try as much as possible to justify the laws we propose, and in particular we test them in light of physical experiments and in light of available natural data. We subsequently integrate these laws into a numerical code, TopoSed, that predicts the macroscale evolution of the landscape under different spatial and temporal uplift and climate scenarios, as well as the sedimentary and exhumation

record left by this evolution. Finally, we perform a series of sensitivity tests on the code to discuss the potential and limits of our approach for estimating paleotopographies and paleouplift rates. This may be particularly relevant to extract quantitative constraints from the sedimentological and paleogeographical records to construct reliable estimates of the Earth's past topography, which, in turn, could be of great use for other issues related to global geodynamics, in particular for constraining past tectonic events and potentially past mantle dynamics [e.g., Conrad and Gurnis, 2003].

## 2. Geomorphic Processes Over Large Spatial and Temporal Scales

### 2.1. Upscaling Elementary Processes

[6] We propose to develop a model that integrates elementary processes over unit spatial and temporal scales of ~100 km and ~1 Ma, respectively. Our approach is based on the assumption that there exists a link between large-scale gradient in topography ( $|\delta H/\delta x|$ , where  $H$  is average regional topography at a ~100 km scale and  $x$  is horizontal distance) and the “true” (i.e., sub-kilometric scale) relief ( $r$ ) that is usually considered to control erosion at the scale of fluvial processes [Ahnert, 1970; Ohmori, 2003; Summerfield and Hulton, 1994]:

$$r = \beta \left| \frac{\delta H}{\delta x} \right| \quad (1)$$

[7] To test this hypothesis, we use the global continental topographic data set GTOPO30 (<http://edc.usgs.gov/products/elevation/gtopo30/gtopo30.html>) to quantify if such a relationship exists on today's Earth topography. We divide the continental surface of the Earth in equal size triangles of length  $l_i$  and compute the average topography in each triangle, the large-scale gradient in topography, and the local relief taken here as the difference between the maximum and minimum altitudes within each triangle. The two latter computed fields are displayed on Figure 3 and show a high degree of correlation: local relief is maximum in regions of high gradient in average altitude (i.e., the edge of plateaus or high mountain ranges), and vice versa. We perform a simple linear regression between these two parameters over the Earth's surface. The resulting correlation coefficients are given in Table 1 as a function of the grid resolution  $l_i$ . The results suggest that the link between mean topographic



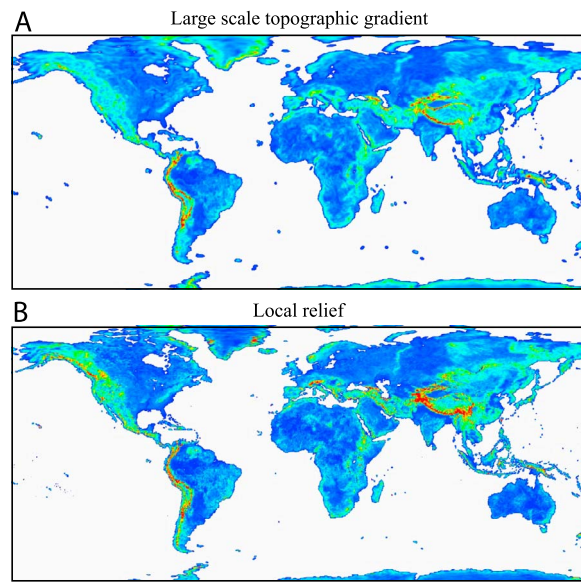


**Figure 3.** (a) Large-scale topographic gradient and (b) local relief of present-day Earth's topography. These data are calculated from GTOPO30 elevation data for equal size triangular cells with a length of 75 km. The color scale goes from blue (low) to red (high) values. We do not provide scalar bars because we only wish to evidence the geographical correlation between the two fields. Note that local relief may be anti-correlated with altitude, in particular in the interior of high continental plateaus (Tibet, South Africa, etc.).

gradient and relief exists and that it is best observed at a scale of up to  $\sim 100$  km. These results also indicate that this link does not strongly depend on length scale, as long as it does not exceed  $\sim 100$  km. This simple relationship suggests that a first-order parameterization of large-scale topographic evolution may be derived from large-scale topographic gradient, as proposed hereafter. It should be noted that local relief and gradient in mean topography can be anti-correlated with elevation such as in the case of high elevation but low relief plateaus (Figure 3).

[8] Sediment production (by bedrock erosion) and transport are treated here separately. We discretize

**Table 1.** Proportionality  $\beta$  and Correlation Coefficient R Between Large-Scale Gradient  $|\delta H/\delta x|$  and Local Relief  $r$  of Present-Day Global Topography<sup>a</sup>

	$l_t$			
	35 km	75 km	150 km	300 km
$\beta$ (m)	$8.02 \times 10^3$	$1.60 \times 10^4$	$3.03 \times 10^4$	$5.68 \times 10^4$
R	0.84	0.82	0.80	0.77

<sup>a</sup>See Figure 3. The correlation is determined for different dimensions  $l_t$  of the triangular cells used to discretize topography.

**Table 2.** Parameters Used to Describe the Macroscale Evolution of the Landscape, and Their Physical Dimension

Parameter	Dimension <sup>a</sup>	Description
$H$	L	mean altitude
$B$	L	mean bedrock altitude
$S$	L	mean sediment thickness
$S_c$	L	critical sediment thickness
$l$	L	dimension of a cell
$U$	$L T^{-1}$	uplift rate
$E$	$L T^{-1}$	bedrock erosion rate
$p$	$L T^{-1}$	runoff (or precipitation) rate
$k_e$	$L^{-1}$	coefficient of erodability
$\tau$	T	characteristic erosion time
$\gamma$	-	density ratio of sediments to bedrock
$\bar{q}$	$L^3 T^{-1}$	sediment flux (in or out of a cell)
$C$	$L^3 T^{-1}$	transport capacity
$k_f$	-	transport coefficient
$Q_w$	$L^3 T^{-1}$	water discharge
$s$	-	regional slope
$A$	$L^2$	upstream area
$H_f$	L	mean altitude of the fan apex of Babault et al. [2005]
$H_{feq}$	L	mean altitude of the fan apex at equilibrium of Babault et al. [2005]
$\tau_f$	T	time constant of fan evolution of Babault et al. [2005]
$r$	L	local topographic relief
$\beta$	L	proportionality coefficient between local relief and large scale topographic gradient

<sup>a</sup>L, length; T, time; dash, dimensionless.

a continental surface in a number of cells of dimension  $l$  of  $\sim 100$  km, characterized by a set of uniform macroscopic morphologic, tectonic and climatic properties (Figure 2). Table 2 lists the different parameters and their physical dimensions, as used in our formalism. The mean elevation ( $H$ ) of a cell depends on the altitude of bedrock ( $B$ ) and on the thickness of sediments ( $S$ ) above bedrock:

$$H = B + S \quad (2)$$

[9] It is important to restate here that the details of natural landscapes are not accounted for in our model. The parameters  $H$ ,  $B$  and  $S$  do not capture the intracell details of landscapes (channels, hill-slopes, etc.) but rather reflect a simple mass budget over a cell between uplifted bedrock, bedrock erosion and sediment transport (Figure 2). Within a cell, various situations could be envisaged where, for example, sediments would be depositing in parts of the cell while, over the same time period, a network of river channels would incise into bedrock. But, as defined here,  $S$  reflects the total volume of available sediments as if uniformly spread over bedrock, and  $B$  the mean elevation of bedrock.



## 2.2. Sediment Production and Transport Over Continental Scales

[10] We consider that bedrock erosion and sediment transport are driven by the potential energy of a cell as related to its altitude above base level, and that erosion and transport operate as a function of the amount of available water, i.e., runoff or precipitation minus evaporation. The sediment production rate ( $E$ ) should integrate both mechanical erosion and chemical weathering. However, because several aspects of chemical weathering are still poorly constrained, we only take into account mechanical erosion of bedrock. First, we postulate that there exists a linear relationship between bedrock erosion rate,  $E$ , and gradient in large-scale topography:

$$E = \frac{\Delta H}{\tau} \quad (3)$$

where  $\Delta H$  is the difference in elevation of the cell with its neighbor in the direction of regional slope (approximately large-scale topographic gradient), and  $\tau$  represents an erosion time scale. Each adjacent cell in the direction of steepest descent is viewed as a local base level (Figure 2), so as to account for the potential existence of endoreic systems and for the effect of piedmont aggradation on the dynamics of the landscape [Babault *et al.*, 2005; Carretier and Lucazeau, 2005; Pelletier, 2004]. A similar macro-scale formalism has already been proposed in the literature [e.g., Milliman and Syvitski, 1992; Ohmori, 2003; Pazzaglia and Brandon, 1996; Pinet and Souriau, 1988; Summerfield and Hulton, 1994], but in the particular case where base level corresponds to sea level ( $\Delta H = H$ ). Erosion is also expected to depend on some climatic parameter and on lithology. We then propose to implement this dependence within the erosion time scale  $\tau$ , so that

$$\tau = \frac{1}{k_e p} \quad (4)$$

where  $p$  is runoff, and  $k_e$  is rock erodability [e.g., Bonnet and Crave, 2006; Davy and Crave, 2000; Kooi and Beaumont, 1996; Summerfield and Hulton, 1994]. The erosion time scale  $\tau$  therefore appears as a characteristic parameter of a cell representing how easily it will erode in response to large scale topographic gradients.

[11] Because erosion may be inhibited by bedrock mantling of sediments, we assume that bedrock erosion only applies when sediments are not locally stored but evacuated downslope. In the case of discrete and partial sediment storage (e.g., fluvial terraces), sediment production may still occur

as a function of the surface of exposed bedrock (Figure 2), which we express as the portion of the cell's surface that would not be covered by a critical sediment thickness  $S_c$ :

$$E = \left( \frac{\Delta H}{\tau} \right) \left( 1 - \frac{S}{S_c} \right) \quad (5)$$

Expression (5) only holds when  $S \leq S_c$ , otherwise erosion is null (i.e., total mantling of bedrock by sediments).

[12] The altitude  $B$  of bedrock varies over time as

$$\frac{dB}{dt} = U - E \quad (6)$$

where  $U$  is rock uplift rate relative to the reference level at  $H = 0$ . The evolution of sediment thickness  $S$  is given by mass conservation:

$$\frac{dS}{dt} = \frac{E}{\gamma} - \frac{\vec{\nabla} \cdot \vec{q}}{l} \quad (7)$$

where  $\gamma = \rho_s / \rho_b$  with  $\rho_s$  and  $\rho_b$  the density of sediment and bedrock respectively, and where  $\vec{q}$  is the solid sediment flux between adjacent sub-regions (dimensions of  $L^3 T^{-1}$ ).  $\vec{\nabla} \cdot \vec{q}$  is positive when the outgoing sediment flux exceeds the incoming flux. We define the sediment transport capacity  $C$  of a cell to its downslope neighbor by the following linear relation [Ludwig and Probst, 1998]:

$$C = k_f Q_w s \quad (8)$$

where  $k_f$  is a dimensionless transport coefficient and  $s$  is the slope between the two cells.  $Q_w$  is the amount of available water:

$$Q_w = \sum p_i A_i \quad (9)$$

where  $A$  is the area of a cell ( $A \sim l^2$ ) and  $i$  relates to each cell upslope from the considered cell. The transport capacity represents the maximum volume of sediments that can be transported downslope. If the volume of sediments exceeds  $C$ , the excess is stored in the cell. This formalism allows for reproducing sediment storage within floodplains, lakes or intracontinental basins (Figures 1 and 2).

[13] Finally, the temporal evolution of  $H$  reflects the balance between bedrock uplift  $U$  and the transfer of sediments at the surface:

$$\frac{dH}{dt} = \frac{d(B + S)}{dt} = U - \frac{\vec{\nabla} \cdot \vec{q}}{l} + E \left( \frac{1}{\gamma} - 1 \right) \quad (10)$$



[14] Our formalism represents a simple view of possible macroscale geomorphic processes, essentially integrating (mesoscale) fluvial erosion and transport. The simplifications assumed here and how they may impact our results are discussed further down.

### 2.3. Testing the Proposed Laws and Calibrating Parameter Values

[15] The laws proposed here for macroscale bed-rock erosion and sediment transport are based on simple intuitive assumptions on how microscale and mesoscale geomorphic processes may be upscaled. Because we want them to be as realistic as possible for the quantitative analysis of the geological record, we test them in light of physical experiments and natural data.

#### 2.3.1. Erosion Law

[16] First, we use the model described above to analyze the evolution of topography and denudation of a purely eroding system ( $\vec{\nabla} \cdot \vec{q} = 0$  and  $S = 0$ ) where base level is set at a constant zero altitude ( $\Delta H = H$ ). If we simplify equation (10) by considering  $\gamma = 1$ , we get

$$\frac{dH}{dt} = U - \frac{H}{\tau} \quad (11)$$

With a zero initial topography, one solution to equation (11) is

$$H = U\tau(1 - e^{-t/\tau}) \quad (12)$$

In these particular conditions only, equation (12) indicates that the erosion time scale  $\tau$  is also the response time of large-scale mean topography  $H$  to tectonic and climatic forcings [Lague *et al.*, 2003]. We test this particular case by comparing our model predictions with the physical experiments of Bonnet and Crave [2003] where different uplift and precipitation rates were applied. When precipitation or uplift rates are abruptly changed during an experiment, equation (11) applies to each portion of the experiment where forcing conditions are stable. In this case, equation (12) may need to be slightly modified to account for a nonzero initial topography. The topographic response time of the experimental landscapes is measured by applying an exponential fit to the evolution of mean topography (Figure 4a). After doing this for all experiments, we find that this response time also corresponds to the erosion time scale  $\tau$  of the model since it allows for reproducing well the evolution of denudation using

equation (3) (Figure 4b). We finally test that the erosion time scale derived from the topographic response time depends mostly on precipitation rate  $p$  as proposed in equation (4) (Figure 4d). Moreover, an inverse relation is found between  $p$  and  $\tau$ . We postulate that the proportionality coefficient of this relation is expected to correspond to lithology ( $k_e$ ). This is somehow confirmed by comparing these experiments performed with silica paste with those obtained in a similar set of experiments carried out with loess [Lague *et al.*, 2003] (Figure 4d). We also find that  $\tau$  is not dependent on uplift (Figure 4c).

[17] We then consider a set of more complex experiments performed by Babault *et al.* [2005], similar to the previous ones except that base level varies with time. The base level is set by fan aggradation (altitude  $H_f$ ) outside the uplifting and eroding zone. In this case,  $\Delta H = H - H_f$  and equation (10) becomes

$$\frac{dH}{dt} = \left(U - \frac{H}{\tau}\right) + \frac{H_f}{\tau} = \left(U - \frac{H}{\tau}\right) + \frac{H_{feq}}{\tau}(1 - e^{-t/\tau}) \quad (13)$$

where we assume that  $H_f$  evolves exponentially with a time constant  $\tau_f$  as suggested by the experiments ( $H_{feq}$  is the steady state altitude of the fan apex). Equation (13) can be partitioned in two terms, the first one corresponding to the characteristic erosive behavior of the system (with a time constant  $\tau$ ), and the second one depending on the evolution of base level (with a time constant  $\tau_f$ ). Steady state cannot be achieved as long as these two terms have not independently reached equilibrium. This means that the longest of the two time scales ( $\tau$  or  $\tau_f$ ) will be that controlling the overall system, as observed by Babault *et al.* [2005]. In the case where the evolution of base level is the limiting controlling factor, Babault *et al.* [2005] noted that the system reached a dynamic equilibrium after a time related to the intrinsic erosional properties of the system ( $\tau$ ), in which erosion balances uplift relative to base level. At dynamic equilibrium or at steady state, we get that  $H_{eq} = U\tau + H_f$ , comparable to that obtained from equation (12) in the case of the previous experiments. Because Babault *et al.* [2005] used the same silica paste as Bonnet and Crave [2003], the same coefficient of erodability  $k_e$  should apply (Figure 4d). From this value and that of the precipitation rate used in these experiments, we calculate an erosion time scale  $\tau \approx 66$  min. However, we rather find that a value of 85 min fits better the observations. This misfit may be related to the scale difference between these two types of

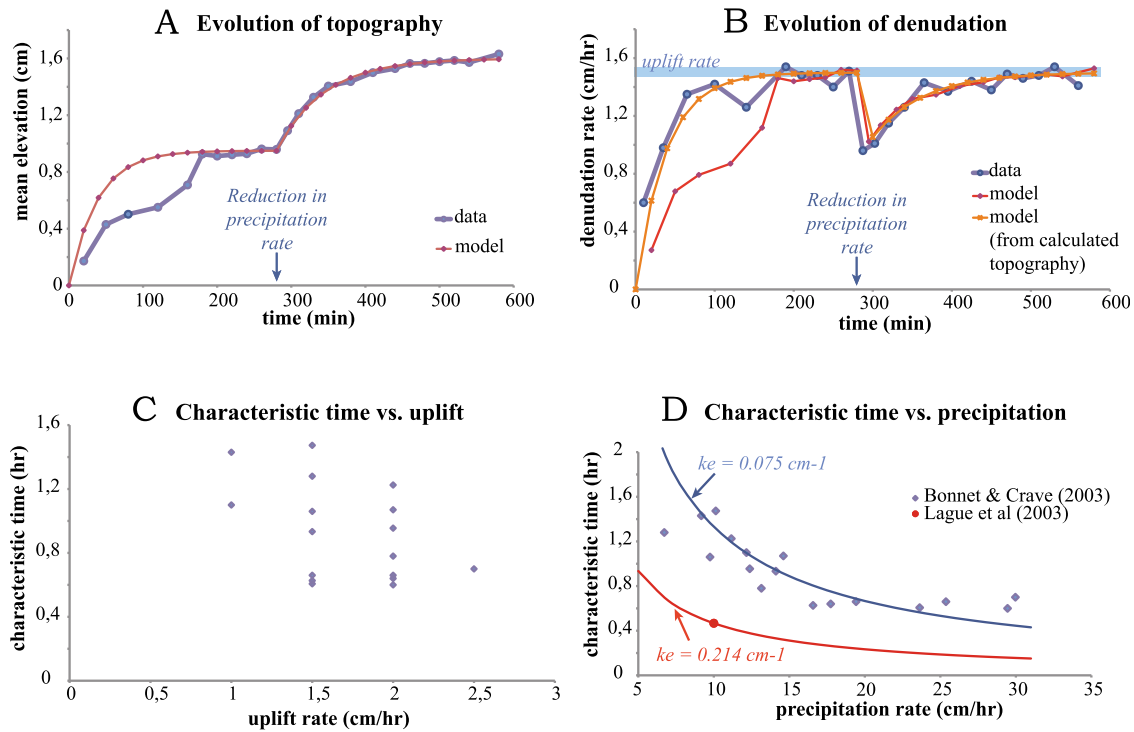


**Figure 4.** Application of the proposed large-scale erosion law to the physical experiments of Bonnet and Crave [2003]. (a) Observed and modeled topography in experiment TC18, where precipitation rate has been halved at 280 min. Modeled topography is calculated from equation (10). Our model fits well the observations except before 200 min, but this misfit is expected to relate to experimental data collection (Figure 4b) rather than to our model. A similar good fit was obtained with other experiments. (b) Observed and modeled denudation rate for experiment TC18. Modeled denudation rate is calculated from equation (2), using the observed (red) or modeled (orange) topography. A significant misfit to the data is observed before 200 min when using observed topography, as in Figure 4a, but disappears when modeled topography is used. This shows that the misfit observed in Figures 4a and 4b is related to the experimental procedure rather than to our model. At steady state, denudation rate equals uplift rate. Similar good fits were obtained with other experiments. (c) Calculated characteristic erosion time  $\tau$  compared to uplift rate for all experiments. (d) Calculated characteristic erosion time  $\tau$  compared to precipitation rate for all experiments. An inverse relation is observed, as expected from equation (3), and indicates a value of  $0.075 \text{ cm}^{-1}$  for  $k_e$ . In the case of the experiments of Lague *et al.* [2003], loess has been used instead of silica paste, and we find a higher erodability of  $0.214 \text{ cm}^{-1}$ . However, this value only relies on one single point.

experiments, but it may also be due to experimental uncertainties. We also find a better fit to the evolution of the fan apex with a value  $\tau_f$  of 175 min rather than that of 247 min proposed by Babault *et al.* [2005]. We then apply equation (13) using these parameter values. A very good fit is obtained between modeled and observed topography (Figure 5a). Finally, we calculate the evolution of the denudation rate as predicted from equation (3), and we find that this equation is also able to reproduce quite well the observations (Figure 5b). These results clearly demonstrate that the simple equations we propose, in particular equation (3), are applicable to the macroscale behavior of experimental landscapes. In particular, the physical models of Babault *et al.* [2005] emphasize the importance of reasoning in terms of relative altitude to base

level, which we have incorporated in our model. We do not pretend that these experiments reflect the complexity of natural systems but they are useful tools to constrain the first order characteristics of the physical processes acting on landscapes.

[18] Ideally, a similar comparison between our model and the evolution of natural systems should be performed. However, we do not know of any data sets comparable to that of these simple physical experiments. Consequently, and in order to rather obtain constraints on the value of the erodability coefficient  $k_e$  in nature, we apply our erosion model on today's Earth topography. We use the triangular discretization of the Earth's surface described above (section 2.1). At each point of the triangulation, we compute the mean altitude  $H$  and



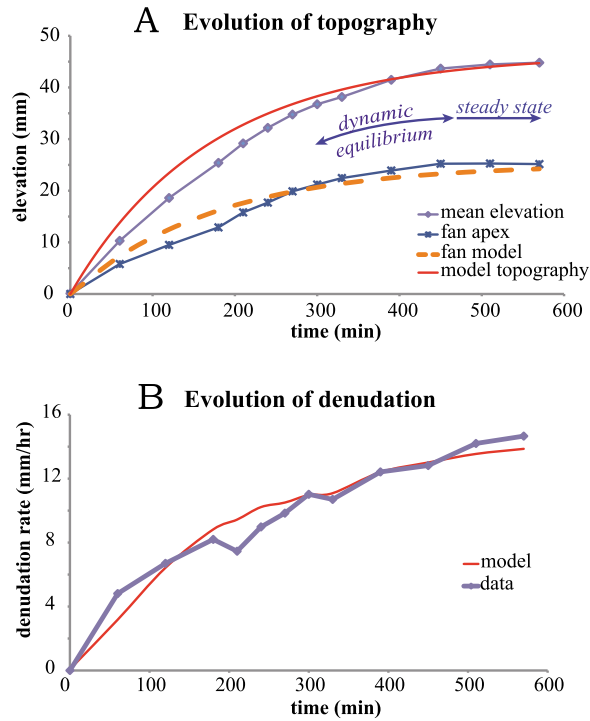


**Figure 5.** Application of the proposed large-scale erosion law to experiment P2 of Babault et al. [2005]. Similar results were obtained with their other experiments. (a) Observed and modeled topography and fan apex, in the case of experiment P2 where dynamic and static equilibriums occur. The fan evolution is fitted with a time constant  $\tau_f$  of 175 min. Modeled topography is calculated from equation (12) using a characteristic erosion time  $\tau$  of 85 min. (b) Observed and modeled denudation rate. Modeled denudation is determined from equation (2) and from the observed topography relative to the fan apex. The characteristic erosion time  $\tau$  is of 85 min.

the large-scale relief value  $\Delta H$ . By multiplying  $\Delta H$  by present-day precipitation rate  $p$  [Hulme, 1992], by bedrock density  $\rho_b$  (2800 kg m<sup>-3</sup>) and by the area of the different cells, we obtain the spatial distribution of predicted sediment mass production (Figure 6a). Using the mean altitude  $H$ , we compute drainage directions at each point, which we then use to compute the geometry of drainage basins (Figure 6b). By integrating sediment mass production over each drainage basin, we obtain the sedimentary mass flux coming out of the mouth of major rivers into the adjacent ocean, assuming that no net deposition takes place on the continental areas (Figure 6c). The predicted and observed locations of major basin outlets match quite well. A linear regression between the computed mass fluxes and those observed in the world's 25 largest rivers [Milliman and Syvitski, 1992]

yields a significant correlation coefficient, while the slope of the correlation between observations and predictions can be used to constrain the value of the coefficient of erodability  $k_e$  (Figure 7a and Table 3). Here we assume that only 50% of the actual eroded bedrock is measured as suspended load at the mouth of major rivers, the rest being transported as dissolved or bed load [Galy and France-Lanord, 2001]. In this way, we obtain a world-averaged value for  $k_e$  of  $1.84 \times 10^{-7} \text{ m}^{-1}$  at a 100 km scale. This value of  $k_e$  may vary in the range of  $1.1 \times 10^{-7}$  to  $2.5 \times 10^{-7} \text{ m}^{-1}$  if we consider that bed

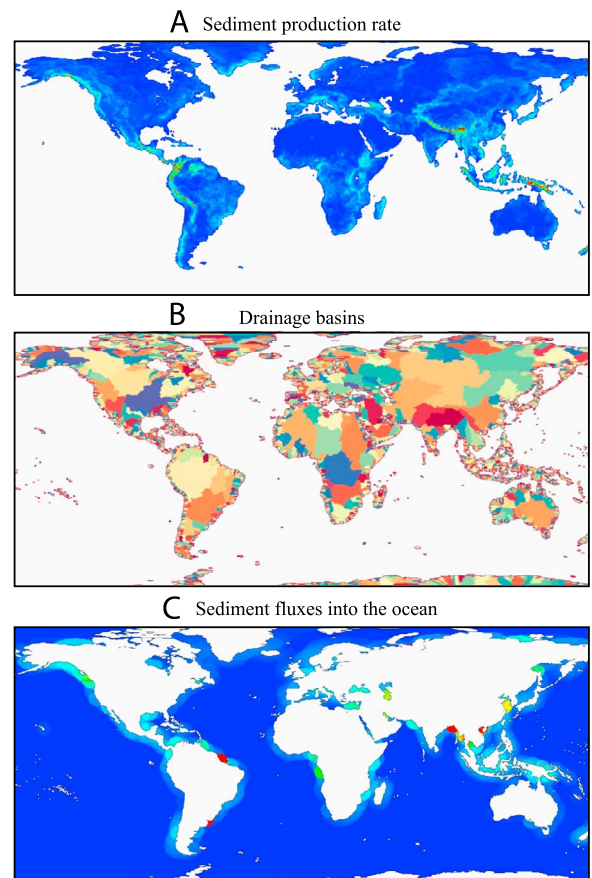


**Figure 6.** (a) Sediment mass production rate computed by multiplying large-scale relief  $\Delta H$  by precipitation rate, bedrock density and cell area; (b) catchment geometries derived from the mean present-day topography estimated on a 100 km triangular mesh; and (c) sediment mass fluxes into the ocean computed by integrating the production function over each continental drainage basin and distributing the resulting sediment load over a 500 km radius from the computed outlet of the basin. We do not provide scalar bars as the absolute value of the computed production and thus deposition functions depends on the value of  $k_e$ . We find a good fit between predicted and observed river sedimentary fluxes for  $k_e = 1.84 \times 10^{-7} \text{ m}^{-1}$  at a 100 km scale.

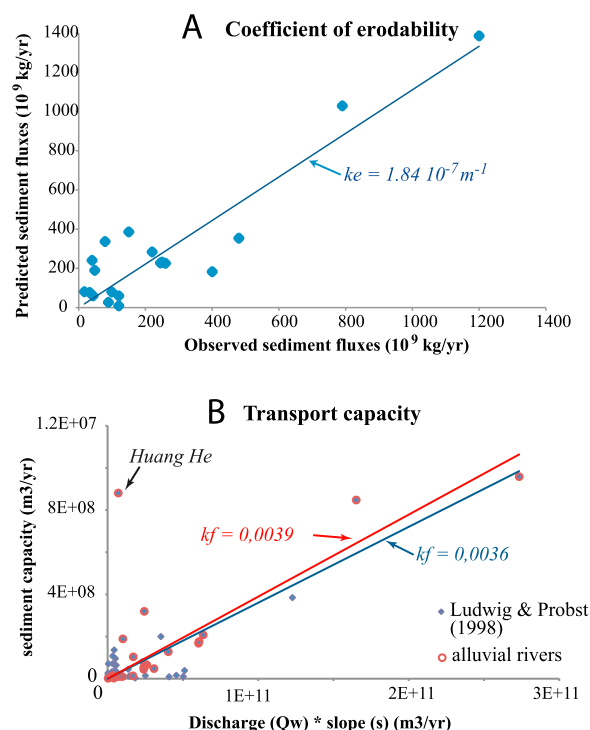


**Figure 7.** Calibration of the erodability and transport coefficients. (a) Present-day predicted versus observed [Milliman and Syvitski, 1992] sediment mass fluxes at the outlet of major rivers (Figure 6) at a 100 km length scale ( $k_e = 1.84 \times 10^{-7} \text{ m}^{-1}$ ). See text for further details on the procedure. (b) Application of equation (8) to the data of Ludwig and Probst [1998]. Sediment transport capacity is determined from sediment load at the mouth of major rivers, calculated assuming that 50% of the total sediment mass is transported as suspended load, and considering a value of  $2500 \text{ kg m}^{-3}$  for  $\rho_s$ . By comparing it to the river discharge  $Q_w$  and to the average drainage slope  $s$ , we get an overall linear relation as proposed from equation (8) (blue line), with a transport coefficient  $k_f$  of 0.0036. Red circles indicate the rivers for which Pinet and Souriau [1988] found evidence of sediment storage within the drainage basins. In this case, the dispersion in the data is slightly reduced, and we get a similar transport coefficient  $k_f$  of 0.0039 (red line). Only one river, the Huang He, appears particularly far from this general trend.

load represents 30% [Dadson *et al.*, 2003] to 70% [Meunier *et al.*, 2006] of the total sediment flux. This demonstrates that large-scale topography can be used to predict the first-order geometry of continental watersheds, except in regions of low topographic relief such as northwestern Africa or central Australia, or except for the geometric details of small high-gradient mountain catchments (Figure 6b). This is the reason why the data from these small rivers has not been used in our calibration, although their contribution to the total global sediment flux

into the oceans is far from negligible [Milliman and Syvitski, 1992]. More importantly, our result confirms the applicability of our first-order parameterization of large-scale continental erosion. It is worth noting too that the correlation between measured and predicted sediment fluxes holds, to first order, for most investigated rivers, independently of their geological and lithological contexts, of the extent of alluvial plains, of their total drainage area (e.g., Amazon versus Choushui) or of the eventual human impact on their sediment load (e.g., HuangHe). Also, it is to note that alluvial plains where sediments are trapped in nature show a low-gradient topography, so that their contribution to calculated sediment fluxes is likely to be negligible. Finally, we find that the erodability coefficient is scale-dependent (Table 3), mostly because the relationship between local relief and regional elevation gradient is also scale-dependent (Table 1). The value discussed here and used hereafter is therefore only valid for cell dimensions of  $\sim 100 \text{ km}$ .

[19] To further test our approach, we make use of erosion rates determined on a longer time scale (1 Myr) using cosmogenic nuclides or low-temperature thermochronology. We consider two examples in different geological contexts, and over different spatial scales. First, the Taiwan mountain belt is a young orogen essentially composed of sandstones and black schists [e.g., Beyssac *et al.*, 2007], where high rates of deformation and erosion suggest that topography has rapidly reached steady state [Willett and Brandon, 2002]. Thermochronological data indicate an average erosion rate of  $\sim 3.2 \text{ mm/yr}$  over the last 2 to 3 Myr at least [Simoes *et al.*, 2007]. With a mean altitude of 1200 m above the coastal plains and a modern precipitation rate of  $\sim 3$  to  $4 \text{ m/yr}$ , this example gives values of  $\tau$  and  $k_e$  of  $\sim 4 \times 10^5$  years and  $\sim 7.6 \times 10^{-7} \text{ m}^{-1}$ , respectively. In a different context, the Orange Basin (Namibia - South Africa) is composed essentially of shales, sandstones and dolerites, and does not show significant sediment storage. It has

**Table 3.** Coefficient of Erodability  $k_e$  and Correlation Coefficient R Between Today's Predicted and Observed Sediment Mass Fluxes at the Mouth of Major Rivers<sup>a</sup>

	$l_t$			
	35 km	75 km	150 km	300 km
$k_e \text{ (m}^{-1}\text{)}$	$3.16 \times 10^{-7}$	$2.14 \times 10^{-7}$	$1.43 \times 10^{-7}$	$1.09 \times 10^{-7}$
R	0.89	0.90	0.93	0.87

<sup>a</sup>Observed sediment mass fluxes are from Milliman and Syvitski [1992]. See Figures 6 and 7a. The correlation is determined for different dimensions  $l_t$  of the triangular cells used to discretize present topography.



certainly had a steady topography over the last hundred thousand years, and cosmogenic nuclides indicate catchment-averaged erosion rates of 4 to 48 m Myr<sup>-1</sup> over this period [Summerfield, 2007]. With a mean altitude of ~1240 m and a modern precipitation rate of ~380 mm/yr [Pinet and Souriau, 1988; Summerfield and Hulton, 1994], we get values of ~26 to 310 Myr and ~10<sup>-7</sup> to 8.5 × 10<sup>-9</sup> m<sup>-1</sup> for  $\tau$  and  $k_e$ , respectively. Although different, the  $k_e$  values obtained for these two contexts are overall comparable to that found from present-day topography and river sediment fluxes, despite the various time and space scales considered. Therefore we are confident in the applicability of our approach. The value of 1.84 × 10<sup>-7</sup> m<sup>-1</sup> for  $k_e$  implies characteristic erosion time scales of ~1 Ma to several 10s of Ma at a ~100 km spatial scale, depending on climate. These values should be considered only as lower bounds for the response time of large-scale topography in situations where external forcings other than local climate (tectonics, base level changes, isostatic adjustments, etc.) do not vary, and are consistent with earlier results of Pinet and Souriau [1988].

### 2.3.2. Transport Law

[20] Equation (8) represents a simple linear relation between transport capacity, discharge and regional slope. We do not know of any specific physical experiment that would allow for testing equation (8), and we make the hypothesis that this relationship is realistic because possible nonlinear mesoscale effects would be homogenized when upscaled. In natural large drainage basins where sediment storage may occur, sediment fluxes at the river mouth should reflect transport capacity of the entire fluvial system. We apply this idea to the 60 worldwide basins investigated by Ludwig and Probst [1998], again assuming that only 50% of the sediments are transported as suspended load [Galy and France-Lanord, 2001], and considering a density  $\rho_s$  of 2500 kg m<sup>-3</sup> to correct for the reduced density of suspended load compared to that of bedrock. We then get a correlation coefficient  $R^2$  of 0.55 (Figure 7b). The dispersion in the data is reduced and the correlation gets better when we only consider the 45 basins where sediment storage is likely to take place in alluvial plains according to Pinet and Souriau [1988]. We then get a median value for  $k_f$  of 3.9 × 10<sup>-3</sup>. The only exception to this broad trend corresponds to the HuangHe, which has one of the world's largest measured sediment capacities due to the highly erodible lithologies characterizing its drainage basin and to modern agricultural practices

[Gaillardet et al., 1999; Hay, 1998]. By excluding this river from our analysis, we significantly improve the correlation coefficient ( $R^2 = 0.88$ ) without changing the value of  $k_f$  (Figure 7b). Such a good correlation is very surprising in view of the expected natural variability of such data, in particular because present-day sediment discharge may not represent the long-term capacity of these major rivers [e.g., Kirchner et al., 2001; Meade and Parker, 1985] and because the percentage of bed load may vary from one river to the other. However, it has been shown that rivers with very large alluvial plains, such as most of those considered here, may have the ability to buffer short-term changes in climate and maintain a constant sediment flux at the outlet provided constant upstream tectonic control on sediment production [Métivier and Gaudemer, 1999]. On the other hand, considering that bed load represents 30% [Dadson et al., 2003] or 70% [Meunier et al., 2006] of the total sediment flux only implies variations of  $k_f$  in the range of 2.61 × 10<sup>-3</sup> ( $R^2 = 0.78$ ) to 6.21 × 10<sup>-3</sup> ( $R^2 = 0.83$ ). Despite the good correlation still observed in these cases, it is slightly reduced compared to when 50% bed load is considered. Therefore, we are confident in our analysis of sediment transport capacity and in the derived average value of  $k_f$ , although our approach will need to be refined in the future when more appropriate data will get available.

[21] The comparison between these observational constraints on the present-day erosion of continental areas and the rate of transport by fluvial systems validates our approach (to the first order), which also seems to agree with the results of physical experiments. We recognize, however, that further testing is needed, in particular by considering other “simple” geological settings (i.e., purely erosive or alluvial) of similar dimensions to those envisaged here. In any case, these equations ought to be improved in the future when further constraints on integrated geomorphic systems will become available, either from a conceptual, empirical or observational aspect.

## 3. TopoSed: A Numerical Code Integrating Large-Scale Geomorphic Processes for the Analysis of Sedimentary Data

### 3.1. Implementing TopoSed

[22] We have implemented equations (2) to (10) into a numerical code, TopoSed, that calculates the large-scale response of landscape to tectonic





and climatic forcings in terms of evolving topography, exhumation rate and time-integrated exhumation, paleogeographies, volume of sediments stored on continents or transported into marine basins. TopoSed therefore performs direct calculations, but it has been designed for future use inside an optimization/inversion algorithm. Also, since the proposed equations are likely to evolve in the future as we get a better sense of large-scale geomorphic processes, we have designed it to be modular and easily updatable, and present here a first version of this code, TopoSed-v1.

[23] We have chosen a squared discretization of space, with cells of dimension  $l$ , essentially for simplicity and to achieve a more practical representation of the solution. In this configuration, five directions of transport are possible (i.e., north, east, south and west along the four sides of the cell, in addition to the cell itself if in a local minimum). We use a finite volume approach [Braun *et al.*, 2001] to solve for the conservation of sediment mass, in particular in equation (7), by considering that the integrated value of  $\vec{\nabla} \cdot \vec{q}$  over a cell's surface equals the fluxes of sediment integrated over the cell's contours. Transport direction between adjacent cells is solved by ordering them using the CASCADE algorithm [Braun and Sambridge, 1997], to make sure that the higher cells are solved before the lower ones in terms of bedrock erosion and of sediment transport. A fully explicit time integration scheme is used to solve for the temporal variation of the different variables. For stability, such an approximation requires calculations over time steps that are very small (i.e.,  $\sim 100$  years to 1 kyr) compared to the time scales for which the model has been developed and over which our calculations are performed ( $\sim 1$ –10 Myr). This is a purely numerical issue and avoids the need for solving a large matrix system as would be required by an implicit time integration scheme. The numerical procedure of TopoSed is as follows. The spatial dimension and the mesh size, the total calculation time, the duration of the time steps, the critical sediment thickness  $S_c$ , and other fixed parameters such as bedrock erodability  $k_e$  and transport capacity  $k_f$  are first set. At each time step, the spatial distribution of time-variable parameters, such as tectonic uplift rate  $U$ , precipitation rate or runoff  $p$ , can be provided. The characteristic erosion time scale  $\tau$  is then calculated for each cell. The altitude of bedrock  $B$  is updated from  $U$  and used to recalculate the spatial distribution of mean topography  $H$ . From there, the code determines the directions of steepest descent and orders the cells based on these

regional drainage directions, using the CASCADE algorithm. The amount of available water  $Q_w$  for sediment transport is then estimated from this ordering and from local and upstream precipitation rate  $p$ . Subsequently, bedrock erosion  $E$  is quantified by considering the altitude  $H$  of each cell relative to the adjacent cell in the direction of regional slope, as well as the amount of locally stored sediments. The sediment transport equation is then solved based on the available volume of sediment and on the transport capacity of the cell estimated in the direction of steepest descent. Sediment transport is calculated here according to the previously determined cell ordering, by integrating from the highest to the lowest, so that the total volume of sediments (locally produced + received from upstream cells) is considered for transport. The amount of sediments transported out of the continent is estimated by collecting the sediments transported out toward the margins at each time step. Finally, parameters such as  $H$ ,  $B$  and  $S$  are updated before restarting the computations for the next time step.

### 3.2. Example of Simulation Using TopoSed

[24] Figure 8 shows a simple direct computation of TopoSed. Our objective is here to illustrate how the code can be used to test tectonic scenarios with sedimentary data, and we do not aim at representing any particular geological situation. We choose arbitrarily here to apply our approach on a spatial scale similar to that of the African continent to show how the code applies to very large spatial scales. The grid encompasses a total of 7560 cells with dimensions of  $100 \times 100$  km. The total duration of the simulation is chosen to be 13 Myr, and spatially varying but temporally constant uplift and precipitation rates are considered during this time interval for simplicity. The spatial distribution of uplift and of precipitations is chosen arbitrarily. The same uplift rate is considered for all uplifted areas and two types of climatic zonations are applied. These model inputs are very basic, but any other tectonic or climatic scenarios could have been chosen for illustration. Parameters  $k_e$  and  $k_f$  are set to values of  $1.84 \times 10^{-7} \text{ m}^{-1}$  and  $3.9 \times 10^{-3}$ , respectively (Table 3 and Figure 7). Bedrock and sediment densities are fixed to 2800 and 2500  $\text{kg m}^{-3}$ , respectively. We propose to consider a critical sediment thickness  $S_c$  of 1 m, similar to the thickness of fluvial deposits in most fluvial strath terraces. From these set of input parameters, TopoSed is able to predict the regional evolution of topography, but more importantly it is able to quantify



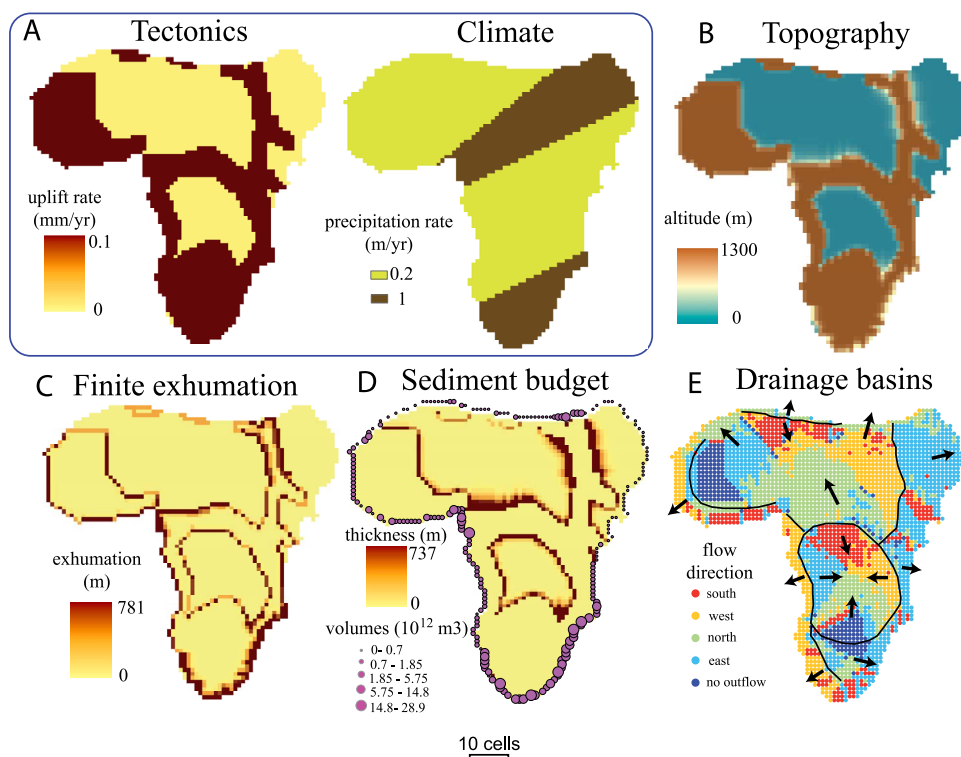


**Figure 8.** Example of a simulation using TopoSed. A continental extent similar to that of Africa is considered as an example. The simulation is performed over 13 Myr, and the grid comprises 7560 cells of 100\*100 km. (a) From a given tectonic and climatic scenario, the code is able to predict (b) continental topography, as well as different other parameters that can be used to test the model inputs against sedimentary and thermochronologic data: (c) finite exhumation, (d) sediment volumes and thicknesses, and (e) geometry of major drainage basins. See text for more details. The flow directions used to predict major drainage basins are taken from the last time step of the 13 Myr long computation.

the associated volume and spatial distribution of sediments trapped in continental plains or transported into marginal basins, the geometry of major drainage systems, the main continental flow directions and continental finite exhumation (Figure 8). All these predictions can be directly compared to sedimentary (sediment budgets, paleogeographic maps, etc.) or thermochronology data. It is to note that the sediment budgets given in Figure 8 are for non-compacted thicknesses or volumes. Because, the main sediment delivery points to the ocean may not be well defined geographically at such spatial scales, in particular in regions of low topographic gradient (Figures 3a and 3b), we do not show them in Figure 8. We rather propose to compare predicted and actual sediment volumes transported to the margins not at a specific outlet but integrated over an entire depositional basin, following the approach of Rouby *et al.* [2009].

[25] This simple simulation illustrates how TopoSed works. If climatic conditions are known, the results

of TopoSed can in principle be used to quantitatively test different tectonic scenarios with more complex spatial and temporal uplift functions, as well as the resulting paleotopographies in light of available geologic records. Input parameters are here very simple and few, except for the spatial distribution and temporal evolution of the forcing parameters (uplift and climate). This is why we propose in the future that TopoSed be incorporated into an optimization (inversion) procedure to extract meaningful and robust estimates of paleotopography from the relevant geological (and mostly sedimentary) record. The scope of our present study is not to perform these inversions but to provide the guidelines and the numerical tools for such investigations. It is clear that the real limit of such approach will not reside in the numerical procedure but rather in the temporal and spatial resolution of the data that will be available in terms of paleoclimates and paleogeographies. It is to note that the simulation illustrated in Figure 8 lasts ~45 min on a regular laptop, essentially because of

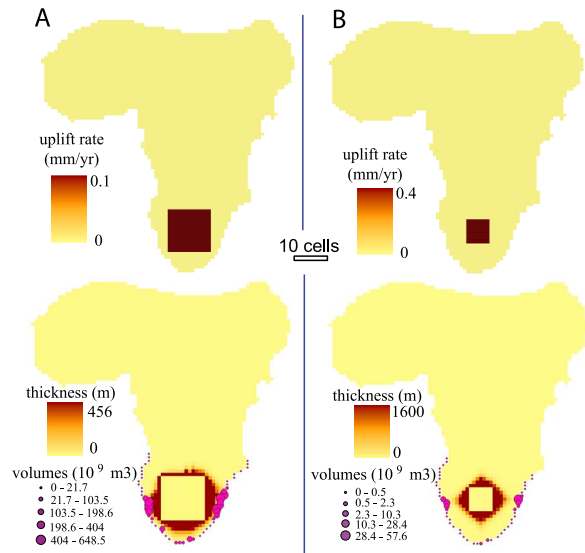


**Figure 9.** Testing the sensitivity of the predictions of TopoSed to different spatial distributions of the same tectonic input. Two cases are considered: (a) 0.1 mm/yr uplift over a wide zone ( $12 \times 12$  cells) and (b) 0.4 mm/yr uplift over a narrower area ( $6 \times 6$  cells). Other parameters (duration, climate, etc) are those of Figure 8. These two examples lead to sediment budgets (thicknesses on continent, fluxes at the margins) that differ by one order of magnitude.

the huge extent of the continental surface considered and the small size of the time steps.

## 4. Discussion

### 4.1. Sensitivity of Model Predictions to Parameter Uncertainties

[26] In this section, we test the sensitivity of the model predictions to model parameters to obtain a good sense of the strengths and limits of our approach, and in particular to better appreciate how well paleouplift rates and/or paleotopographies are expected to be numerically resolved from sedimentary records.

[27] We first consider two cases similar to the reference numerical experiment illustrated in Figure 8 (same duration, climate, etc.), but with different tectonic scenarios (Figure 9). The same space-time integrated tectonic forcing (= uplift rate  $\times$  uplifted area  $\times$  duration of uplift) is applied in either case, but on regions with sizes that differ by a factor 4 (and therefore with uplift rates that differ by the inverse). As expected, we find that the total sediment budget is similar in either case. However, the results show significant differences (up to 1 order of magnitude) in the spatial distribution of sedi-

ments, with greater volumes transported toward the margins (and therefore smaller thicknesses preserved on the continent) in the case of a spatially wider but lower uplift. This indicates that the total sediment budget depends essentially on the integrated tectonic forcing but that its spatial distribution is sensitive to that of uplift.

[28] The details of the temporal variability of parameters (sub-Myr scale) such as uplift or climate are unlikely to be captured with a model designed to operate over longer periods of time and commonly constrained by observations that have a low spatial and temporal resolution. Consequently mean parameter values, averaged over several Myr,

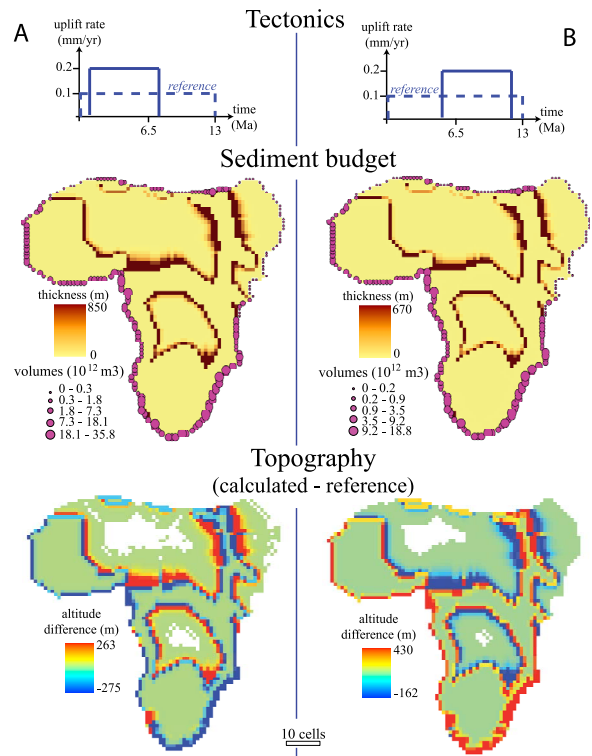


**Figure 10.** Testing the sensitivity of the predictions of TopoSed to different temporal scenarios of uplift, relative to an average scenario with constant tectonics as in Figure 8 (top, dashed line). The spatial distribution of uplift and all other parameters are those of Figure 8. Two cases are considered (top, continuous lines), with twice the uplift rate of the reference scenario but over half the calculation time: uplift (a) at the beginning and (b) at the end of the simulation. Model results are given in terms of sediment thicknesses (on continent) and volumes (at the margins), as well as in terms of differences in topography relative to that predicted in Figure 8 (calculated topography – reference topography). Sediment flow directions are not shown here but are identical to those predicted in the reference scenario.

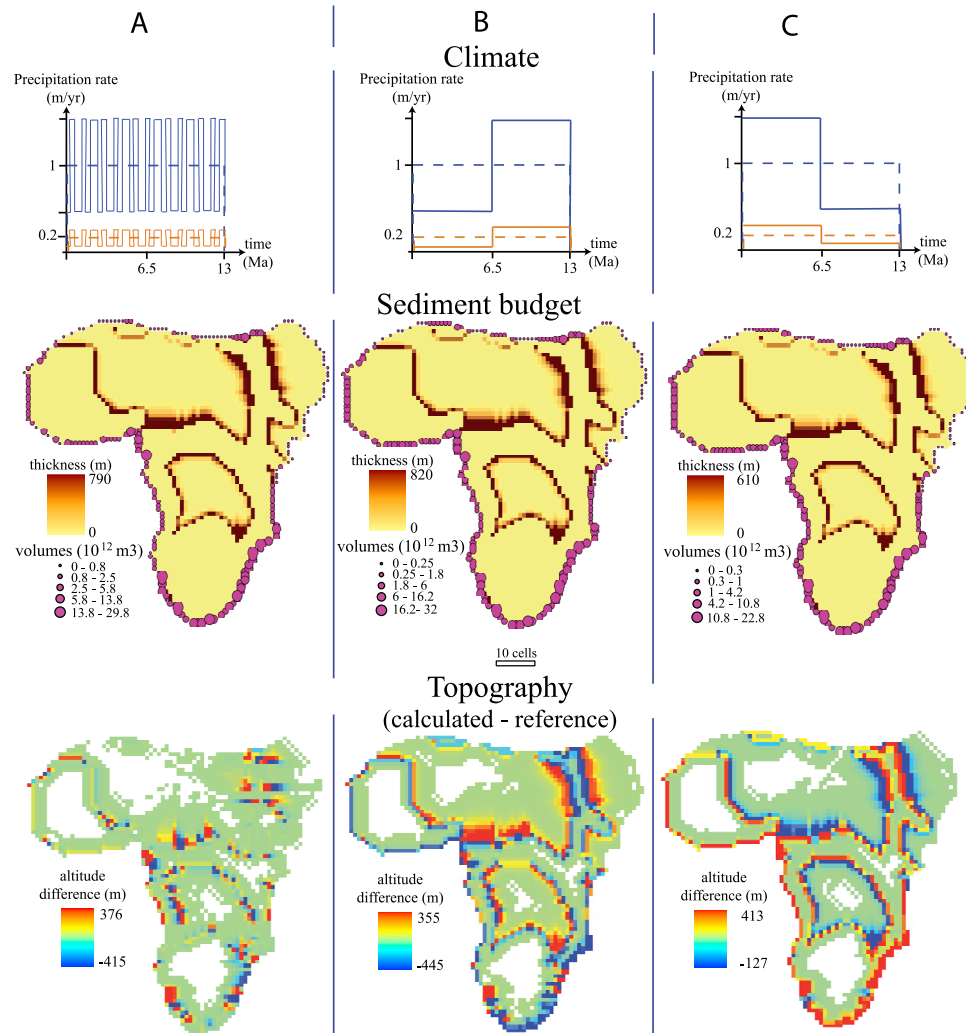


**Figure 11.** Testing the sensitivity of the predictions of TopoSed to different temporal climatic scenarios (top, continuous lines), that average to the reference constant scenario of Figure 8 (top, dashed line). The red lines correspond to the precipitation rates applied to the more arid regions, and the blue ones correspond to the more humid regions (Figure 8). Three cases are considered: (a) climatic oscillations with changes every 100 ka (periodicity not to scale in the diagram), (b) dryer to more humid conditions, and (c) more humid to dryer conditions over time. Model results are given in terms of sediment thicknesses (on continent) and volumes (at the margins), as well as in terms of differences in topography relative to that predicted in Figure 8 (calculated topography - reference topography). Sediment flow directions are not shown here but are identical to those predicted in the reference scenario.

are to be used in direct or inverse calculations. To test how this affects paleouplift rates or paleotopographies calculated from sedimentary data using TopoSed, we perform a series of tests comparing model results obtained using forcing parameter values averaged over the whole simulation with those obtained when incorporating some variability in these parameters (Figures 10 and 11). Our average reference scenario is that depicted on Figure 8, and synthetic data are obtained here with simulations that differ only in the temporal variability of uplift or climate. We first test the sensitivity to different temporal distributions of uplift

(Figure 10), with high uplift rates at the beginning or at the end of the simulation time. We find that the sediment budget is, in either case, of the same order of magnitude and is not significantly different from that of the reference scenario. Sediment thicknesses and volumes are slightly higher when high uplift rates are applied early in our calculations. This is because in this case the created topography keeps being eroded even in the absence of any tectonics at the end of the calculations, whereas there has not been enough time for as much bedrock erosion in the other case. This is also reflected in the topography when compared to the

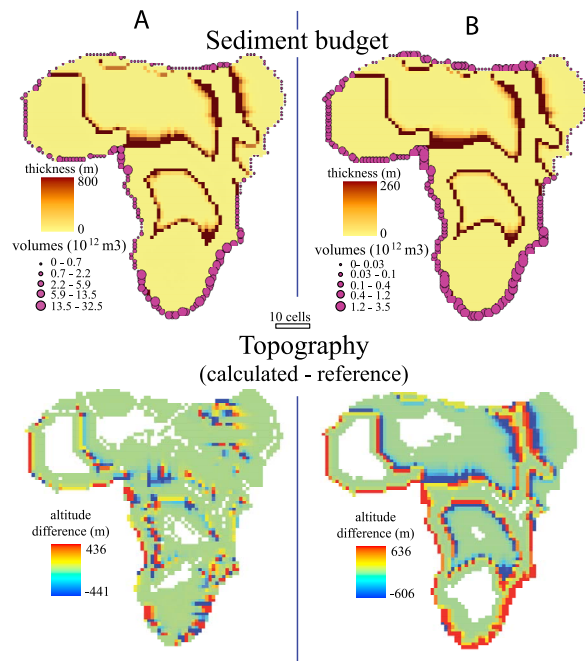


**Figure 12.** Testing the sensitivity of the predictions of TopoSed to different values of the erodability coefficient  $k_e$  that differ by one order of magnitude relative to the value proposed from present-day sediment fluxes in major rivers (Table 3 and Figure 7a): (a) with  $k_e = 1.84 \times 10^{-6} \text{ m}^{-1}$  and (b) with  $k_e = 1.84 \times 10^{-8} \text{ m}^{-1}$ . All other parameters are those considered in the reference model of Figure 8. Model results are given in terms of sediment thicknesses (on continent) and volumes (at the margins), as well as in terms of differences in topography relative to that predicted in Figure 8 with  $k_e = 1.84 \times 10^{-7} \text{ m}^{-1}$  (calculated topography - reference topography). Sediment flow directions are not shown here but are identical to those predicted in the reference scenario.

average scenario, with altitudes slightly higher in sedimentary basins and lower at the margins of eroded areas in the case of an early uplift (and the inverse is true in the other case). Topographic differences are at most of  $\sim 400 \text{ m}$ . Altogether, these different scenarios should lie within usual data uncertainties [e.g., *Rouby et al.*, 2009] and should therefore be hard to distinguish from actual data. We then test the sensitivity of the system to variable precipitation rates over time, with the same spatially and temporally integrated precipitation as that of Figure 8 (Figure 11). The geography of the climatic zones (humid and dry) is kept identical. Three cases are considered: (1) rapid climatic oscillations (every 100 ka), (2) long-term variations (half the calculation time) with a transition from dryer to more humid conditions, and (3) same as case 2 but with a transition from more humid to dryer conditions. In the case of rapid climatic os-

cillations, sediment budgets are identical to those of the average scenario. The predicted topography is almost identical, except in some areas where differences may be of up to  $\sim 400 \text{ m}$ . These regions of discrepancy are not particularly coherent with areas of erosion or sedimentation and may represent the natural uncertainty on model results. In the case of long-term climatic variations, sediment volumes and thicknesses are of the same magnitude as those of the average scenario, although they tend to be greater when climate is more humid at the end of the simulations. This is because topography (and therefore regional slopes) is already high by the time climatic conditions get more erosive. Topography differs by up to  $\sim 400 \text{ m}$  relative to the reference scenario of Figure 8, with higher elevations in basins (because more sediments are collected) and lower elevations in eroded areas (because of more intense exhumation). The inverse is true in the case of initial humid conditions. Altogether, these three cases should be hardly distinguishable from that of Figure 9 based on sedimentary data alone.

[29] Finally, we test the sensitivity of model predictions to various parameters such as bedrock erodability  $k_e$ , transport constant  $k_f$  and critical sediment thickness  $S_c$ . We vary these parameters by one order of magnitude relative to the values used in Figure 8, which is well above the expected variability of parameters such as  $k_e$  or  $k_f$ . In the case of low erodability  $k_e$ , sediment volumes at the margins are lower by one order of magnitude and the differences in topography are of up to  $\sim 600 \text{ m}$  (Figure 12b). The model seems much less sensitive to higher erodability values, since sediment thicknesses and volumes are similar to those of Figure 8. Differences in topography are in this case of up to  $\sim 400 \text{ m}$  but with no clear coherence between eroding or depositing regions (Figure 12a). Lower transport efficiency has an effect similar to that of lower bedrock erodability (Figure 13b). Model results seem to be quite sensitive to higher values of  $k_f$ , with slightly higher sediment budgets relative to the reference model, but with a much widespread sediment distribution (Figure 13a). A higher transport efficiency leads to more efficient evacuation of the sediments out of the eroding regions, and therefore increases erosion. This is clearly shown in the topographic differences (up to  $\sim 650 \text{ m}$ ) in comparison with the reference experiment, with lower eroding regions and with higher and larger sedimentary basins when  $k_f$  is high (Figure 13a). The critical sediment thickness  $S_c$  has no particular impact on the sediment budget predictions



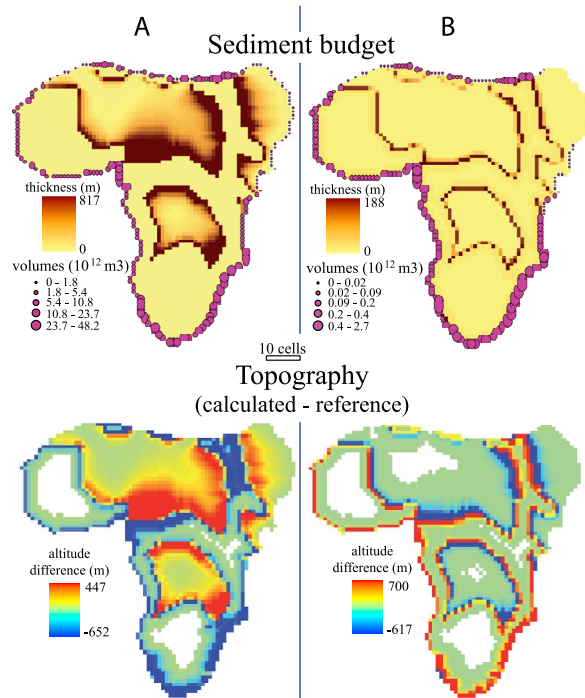


**Figure 13.** Testing the sensitivity of the predictions of TopoSed to different values of the transport coefficient  $k_f$  that differ by one order of magnitude relative to the value found by sediment fluxes at the mouth of present-day major rivers (Figure 7b): (a) with  $k_f = 3.9 \times 10^{-2}$  and (b) with  $k_f = 3.9 \times 10^{-4}$ . All other parameters are those considered in the reference model of Figure 8. Model results are given in terms of sediment thicknesses (on continent) and volumes (at the margins), as well as in terms of differences in topography relative to that predicted in Figure 8 with  $k_f = 3.9 \times 10^{-3}$  (calculated topography – reference topography). Sediment flow directions are not shown here but are identical to those predicted in the reference scenario.

(Figure 14). Differences in topography relative to that of the reference model may be of up to  $\sim 300$  m, but these differences do not show a particular spatial coherence and are probably related to model intrinsic uncertainties.

[30] These tests are not exhaustive but provide an idea on the numerical strengths and limitations of TopoSed. Provided that good constraints on the erodability and transport coefficients are available, the finite sediment budget is essentially sensitive to the space and time integrated tectonic forcing (Figures 9 and 10), and the spatial distribution of these sediments (mostly margins versus continent) to the spatial distribution of uplift (Figure 9). These results follow the idea of *Bonnet and Crave* [2003] and *Whipple and Meade* [2006] that finite denudation and sedimentation should equilibrate with

tectonics. They also imply that sedimentary fluxes can in principle be used to retrieve paleouplift rates, even over very extensive continental areas provided a certain spatial resolution of the data. In practice, because the total volume of sediments is needed, sedimentary fluxes should be considered over the whole depositional areas and not only onland or over the platform of continental margins, as recently suggested by *Rouby et al.* [2009]. In contrast, topography appears more sensitive to the details of most of the input and forcing parameters such as tectonics, climate, and erodability or transport efficiency. In the previous tests, this is essentially the case in regions affected by erosion or sedimentation, where “errors” associated with the variability of each parameter taken separately are at most of  $\sim 600$  m (Figures 10–14). In practice, the uncertainty in topography related to long-term temporal variations in uplift (Figure 10) or in climate (Figure 11), can be reduced and even elimi-

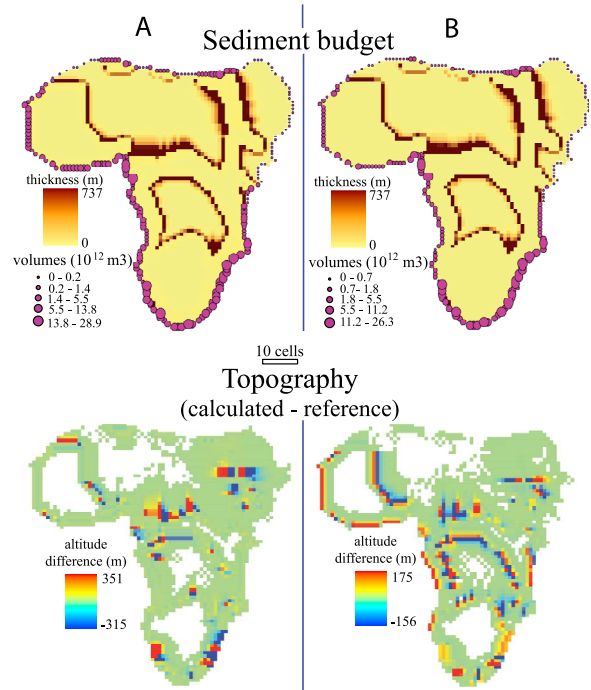


**Figure 14.** Testing the sensitivity of the predictions of TopoSed to different values of the critical sediment thickness  $S_c$  that differ by one order of magnitude relative to the value chosen in the reference model of Figure 8: (a) with  $S_c = 10$  m and (b) with  $S_c = 0.1$  m. Model results are given in terms of sediment thicknesses (on continent) and volumes (at the margins), as well as in terms of differences in topography relative to that predicted in Figure 8 with  $S_c = 1$  m (calculated topography – reference topography). Sediment flow directions are not shown here but are identical to those predicted in the reference scenario.



nated if the calculation time is defined in relation to local geological constraints on long-term tectonic or climatic events, rather than being established simply by following global stratigraphic limits or by taking an arbitrary duration. When a long period of time is considered, calculations should be subdivided into several sub-periods, whose durations can vary according to geological knowledge on tectonics or climate. In contrast, short-term climatic oscillations can induce topographic errors of up to ~400 m with respect to the average reference scenario (Figure 11), and such particular details on climate are unfortunately elusive to obtain for the geological past. The critical sediment thickness  $S_c$  was fixed to a geologically reasonable value, but this choice was somehow arbitrary. Possible variations on this parameter may also generate an uncertainty of up to ~300 m in topographic predictions (Figure 14). Finally, variations in  $k_e$  or  $k_f$  by one order of magnitude have significant implications in most model predictions (sediment budgets as well as topography). However, we believe to have reasonable estimates for these parameters (Figure 7 and Table 3) and we do not presently have any particular evidence for varying them by up to one order of magnitude. Note that we did not show on Figures 10–14 the predicted drainage basins and the main continental flow directions because these were identical to those of the reference scenario of Figure 8e.

[31] As a conclusion, although there is good hope to retrieve paleouplifts from sedimentary data provided caution is exercised in selecting the duration of the simulations, paleotopographies are not expected to be resolved at a resolution better than ~500 m. This may be problematic to further constrain paleouplifts on continents, since the topography generated over a certain time interval corresponds to the initial conditions in terms of regional slopes (and therefore in terms of sediment production) for modeling a subsequent period of time. Uncertainties in predicted topography are therefore expected to generate errors in calculated uplifts, and these errors would propagate from one simulation to the next one. To compensate for this, there may be the need for a constant feedback between model predictions and sedimentary data at each time step considered. As an example, regional slopes implied by the predicted topography could be tested in light of those that could be derived from the sedimentary record of ancient fluvial systems [e.g., *Heller and Paola*, 1989; *Padgett and Ehrlich*, 1976], although the calibration between river hydrodynamics and slope is not straightfor-

ward and needs to be further investigated [e.g., *Paola and Mohrig*, 1996; *Schumm and Khan*, 1972; *Schumm*, 1985].

## 4.2. Interpretation of Modeled Uplift Rates

[32] In the current version of TopoSed, calculations are performed over emerged continental areas only. Sea level appears in fact as a reference level, in particular because it sets the lowermost base level for erosion, and its position over the continents can be known in the past from sedimentary records (e.g., shorelines). Uplift rates are also considered relative to this reference level (equation (6)). However, to extract absolute uplift rates, in the sense of vertical displacement of rocks relative to the geoid [*England and Molnar*, 1990], one would need to correct the predicted values for sea level fluctuations over geological times. The revised eustatic chart of *Miller et al.* [2005] could be used for such corrections.

[33] One should also be reminded that our approach is purely kinematic. To this extent the total uplift rate modeled using TopoSed incorporates rock vertical displacements related to both tectonic forcing and the corresponding isostatic adjustment.

## 4.3. Limitations of TopoSed Related to the Proposed Erosion and Transport Laws

[34] The erosion and transport laws introduced in this first version of TopoSed represent possible processes operating over large spatial and temporal scales, essentially inspired from our present view of mesoscale fluvial processes. We did not specifically introduce an erosion threshold as observed in natural systems [*Pinet and Souriau*, 1988] or in physical experiments of landscape relaxation [*Lague et al.*, 2003]. However, we notice in all above simulations (Figures 8–14) that the system “naturally” gets to a threshold since regions below a certain altitude usually correspond to areas of deposition and not of erosion. This threshold seems to depend on parameters such as  $k_e$  or  $k_f$  (Figures 12–13) and a realistic altitude of ~600 m is attained (Figures 8, 10, 11, and 14) for reasonable parameter values. This is certainly related to the fact that TopoSed is not a purely erosion model: it incorporates sediment deposition and transport out of the uplifted regions, and bed-rock erosion is limited by the efficiency of the system to evacuate these sediments (equation (5)). In addition to that, the erosion law proposed in equations (3) and (5) suggests that the sedimentary response of the landscape to any change in base level is immediate. In reality, there may be a delay when



the connectivity of the landscape to the local base level is not complete [Davy and Crave, 2000; Kooi and Beaumont, 1996; Lague *et al.*, 2003] and part of the sediment is stored in low elevation, topographically enclosed areas. This is particularly the case when the time scale of the external forcing is much shorter than the characteristic time scale for erosion  $\tau$ . Lithology ( $k_e$ ) and climate ( $p$ ) are intuitively expected to play some role in the building of the network connectivity, so that the time to achieve connectivity could be proportional to  $\tau$ . One numerical experiment of Kooi and Beaumont [1996] suggests that this time lag could be  $\sim 5\%$  of the  $\tau$  value, and we consider that this is probably within current uncertainties on this parameter. Also, the initial conditions of a real landscape are rarely those of a zero and non-connected topography.

[35] In addition, even though our macroscale erosion and transport laws can be considered intuitively reasonable with respect to mesoscale fluvial processes, they are to some extent over-simplified. The impact of climate on erosion is here simply related to the amount of average precipitations. Climate is indeed characterized by a multitude of parameters other than precipitation that can all impact erosion efficiency [e.g., Ludwig and Probst, 1998]. This is the case of seasonality or extreme events, in particular for arid environments, and is also the case of the vegetation cover. These complexities were not incorporated here because their impact is controversial [Lague *et al.*, 2005] and poorly constrained [Tucker, 2004]. Also, quantifying their significance is certainly elusive for the geological past. Finally, other surface processes such as eolian or glacial erosion and transport are here not accounted for, essentially because their mesoscale contribution is still poorly quantified [Braun, 2006]. Application of the present version of TopoSed to cases for which there is geological evidence of eolian or glacial erosion and transport should therefore be done with caution.

[36] In addition to simplifying physical processes of erosion, our approach neglects the effects of chemical weathering on long-term sediment budgets and predicted topography. Chemical weathering depends on a multitude of factors, such as lithology or climate, but it seems essentially coupled to physical erosion [Gaillardet *et al.*, 1999; Summerfield and Hulton, 1994]. In the case of silicates, a simple power law relation has been proposed between these two processes [Millot *et al.*, 2002] based on data from rivers of the Canadian Shield. We have attempted to introduce this relationship in TopoSed to account for chemical ero-

sion and to apply it to bedrock erosion. However, in doing so, we found that chemical erosion became the most significant process over the long-term, rapidly erasing most of the topography. These results seem unrealistic and are an artifact of the small exponent ( $<1$ ) relating physical erosion to chemical weathering in the equation of Millot *et al.* [2002], in particular because at the short time steps considered for our calculations physical erosion is small ( $<1$  m over 100 ka). This may suggest that, although correlated, physical and chemical erosion do not proceed over the same time scales. In any case, this relation is imperfect in that it only applies to silicates. However, even if a similar relation were provided for other lithologies such as carbonates or evaporites, there would be little hope to constrain the type of eroded bedrock anywhere on continents over the geological past. How neglecting chemical erosion impacts our results is not straightforward: predicted topographies may be simply over-estimated, but they may also be underestimated if sediment budgets used to constrain paleouplifts are in fact underestimated because of the mass loss associated with chemical weathering of sediments during transport and deposition. Further constraints (time constants, macroscale law, etc.) on chemical weathering need to be gathered before being implemented in TopoSed.

[37] In any case, we only present here a first version of TopoSed-v1, and the code is meant to evolve in the future as we get a better quantitative knowledge of these different geomorphic processes and as we can properly upscale them in space and time.

## 5. Conclusion

[38] In this manuscript, we propose a set of simple erosion and transport laws that are based on the up-scaling of mesoscale fluvial processes to large spatial ( $\sim 100$  km) and temporal ( $\sim 1$  Ma) scales. These have been tested in light of physical experiments of landscape evolution and further calibrated using data on present-day sediment fluxes at the mouth of major rivers worldwide. These laws have subsequently been incorporated into a numerical code, TopoSed, that predicts topography, sedimentary fluxes, paleogeographies and exhumation from a given tectonic and climatic scenario. Such a code, coupled to an inversion algorithm, could be used in the future to invert for paleouplift rates and paleotopographies using sedimentary and thermochronological data. Following the idea that sediment fluxes are essentially dependent on tectonic



forcing, in contrast with topography which adjusts to both tectonics and climate, it should in theory be possible to invert for uplift rates. On the other hand, constraining the evolution of regional topography is more subtle and should highly be dependent on the resolution of sedimentary data, but also on the selection of the calculation durations with respect to long-term tectonic or climatic events. To clearly solve for this, a continuous feedback between data and predictions is therefore needed.

[39] One of the strengths of our approach is to incorporate separately both bedrock erosion and transport, which may interact on a complex way at continental scales [e.g., Allen, 2008]. Also, these processes are expected to be scale-dependent, but this issue is resolved by considering a consistent spatial unit (~100 km) in our calculations. A first application of our approach is presently conducted by our group in Geosciences Rennes (France) in the frame of the TopoAfrica project, with focus on the Meso-Cenozoic evolution of the African topography and uplift as recorded in marginal and continental sediments.

## Acknowledgments

[40] This work was motivated by the numerous discussions with D. Rouby, F. Guillocheau and C. Robin (Géosciences Rennes, France), who exposed the difficulties encountered by sedimentologists in quantifying the past evolution of continental surfaces from geological records. This study also benefited from the comments by two anonymous reviewers. We also thank the Editor T. Becker for his contribution to clarifying the manuscript, as well as for his prompt editorial handling. This study was supported by the ANR (Agence Nationale de la Recherche) through a “Chaire d’Excellence Senior” grant attributed to J.B. and through the TopoAfrica Project (PI F. Guillocheau).

## References

- Aalto, R., et al. (2006), Geomorphic controls on Andean denudation rates, *J. Geol.*, **114**, 85–99, doi:10.1086/498101.
- Ahnert, F. (1970), Functional relationships between denudation, relief, and uplift in large mid-latitude drainage basins, *Am. J. Sci.*, **268**, 243–263.
- Allen, P. A. (2008), From landscapes into geological history, *Nature*, **451**, 274–276, doi:10.1038/nature06586.
- Avouac, J. P., and E. B. Burov (1996), Erosion as a driving mechanism of intracontinental mountain growth, *J. Geophys. Res.*, **101**(B8), 17,747–17,769, doi:10.1029/96JB01344.
- Babault, J., et al. (2005), Influence of piedmont sedimentation on erosion dynamics of an uplifting landscape: An experimental approach, *Geology*, **33**(4), 301–304, doi:10.1130/G21095.1.
- Beyssac, O., M. Simoes, J. P. Avouac, K. A. Farley, Y.-G. Chen, Y.-C. Chan, and B. Goffé (2007), Late Cenozoic metamorphic evolution and exhumation of Taiwan, *Tectonics*, **26**, TC6001, doi:10.1029/2006TC002064.
- Binnie, S. A., et al. (2007), Tectonic uplift, threshold hillslopes, and denudation rates in a developing mountain range, *Geology*, **35**, 743–746, doi:10.1130/G23641A.1.
- Bonnet, S., and A. Crave (2003), Landscape response to climate change: Insights from experimental modeling and implications for tectonic versus climatic uplift of topography, *Geology*, **31**(2), 123–126, doi:10.1130/0091-7613(2003)031<0123:LRTCCI>2.0.CO;2.
- Bonnet, S., and A. Crave (2006), Macroscale dynamics of experimental landscapes, in *Analogue and Numerical Modelling of Crustal-Scale Processes*, edited by S. J. H. Buiter and G. Schreurs, *Geol. Soc. Spec. Publ.*, **253**, 327–339.
- Braun, J. (2006), Recent advances and current problems in modelling surface processes and their interactions with tectonics and crustal deformation, in *Analogue and Numerical Modelling Of Crustal-Scale Processes*, edited by S. J. H. Buiter and G. Schreurs, *Geol. Soc. Spec. Publ.*, **253**, 307–325.
- Braun, J., and M. Sambridge (1997), Modelling landscape evolution on geologic time scales: A new method based on irregular spatial discretization, *Basin Res.*, **9**, 27–52, doi:10.1046/j.1365-2117.1997.00030.x.
- Braun, J., et al. (2001), Sediment transport mechanisms on soil-mantled hillslopes, *Geology*, **29**(8), 683–686, doi:10.1130/0091-7613(2001)029<0683:STMOSM>2.0.CO;2.
- Carretier, S., and F. Lucazeau (2005), How does alluvial sedimentation at range fronts modify the erosional dynamics of mountain catchments?, *Basin Res.*, **17**(3), 361–381, doi:10.1111/j.1365-2117.2005.00270.x.
- Conrad, C. P., and M. Gurnis (2003), Seismic tomography, surface uplift, and the breakup of Gondwanaland: Integrating mantle convection backwards in time, *Geochim. Geophys. Geosyst.*, **4**(3), 1031, doi:10.1029/2001GC000299.
- Dadson, S. J., et al. (2003), Links between erosion, runoff variability and seismicity in the Taiwan orogen, *Nature*, **426**, 648–651, doi:10.1038/nature02150.
- Dadson, S. J., et al. (2004), Earthquake-triggered increase in sediment delivery from an active mountain belt, *Geology*, **32**(8), 733–736, doi:10.1130/G20639.1.
- Davy, P., and A. Crave (2000), Upscaling local-scale transport processes in large-scale relief dynamics, *Phys. Chem. Earth*, **25**(6–7), 533–541.
- Dietrich, W. E., D. G. Bellugi, L. S. Sklar, J. D. Stock, A. M. Heimsath, and J. J. Roering (2003), Geomorphic transport laws for predicting landscape form and dynamics, in *Prediction in Geomorphology*, *Geophys. Monogr. Ser.*, vol. 135, edited by P. R. Wilcock and R. M. Iverson, pp. 103–132, doi:10.1029/135GM09, AGU, Washington, D. C.
- England, P., and P. Molnar (1990), Surface uplift, uplift of rocks, and exhumation of rocks, *Geology*, **18**, 1173–1177, doi:10.1130/0091-7613(1990)018<1173:SUUORA>2.3.CO;2.
- Fluteau, F., G. Ramstein, and J. Besse (1999), Simulating the evolution of the Asian and African monsoons during the past 30 Myr using an atmospheric general circulation model, *J. Geophys. Res.*, **104**(D10), 11,995–12,018, doi:10.1029/1999JD900048.
- Gaillardet, J., et al. (1999), Global silicate weathering and CO<sub>2</sub> consumption rates deduced from the chemistry of large rivers, *Chem. Geol.*, **159**, 3–30, doi:10.1016/S0009-2541(99)00031-5.
- Galy, A., and C. France-Lanord (2001), Higher erosion rates in the Himalaya: Geochemical constraints on riverine fluxes,



- Geology*, 29(1), 23–26, doi:10.1130/0091-7613(2001)029<0023:HERITH>2.0.CO;2.
- Galy, V., et al. (2007), Efficient organic carbon burial in the Bengal fan sustained by the Himalayan erosional system, *Nature*, 450, 407–410, doi:10.1038/nature06273.
- Galy, V., et al. (2008), Recycling of graphite during Himalayan erosion: A geological stabilization of carbon in the crust, *Science*, 233, 943–945, doi:10.1126/science.1161408.
- Godard, V., et al. (2006), Numerical modelling of erosion processes in the Himalayas of Nepal: Effects of spatial variations of rock strength and precipitation, in *Analogue and Numerical Modelling of Crustal-Scale Processes*, edited by S. J. H. Buiter and G. Schreurs, *Geol. Soc. Spec. Publ.*, 253, 341–358.
- Hay, W. W. (1998), Detrital sediment fluxes from continents to oceans, *Chem. Geol.*, 145, 287–323, doi:10.1016/S0009-2541(97)00149-6.
- Heller, P. L., and C. Paola (1989), The paradox of Lower Cretaceous gravels and the initiation of thrusting in the Sevier orogenic belt, United States Western Interior, *Geol. Soc. Am. Bull.*, 101, 864–875, doi:10.1130/0016-7606(1989)101<0864:TPOLCG>2.3.CO;2.
- Howard, A. D., W. E. Dietrich, and M. A. Seidl (1994), Modeling fluvial erosion on regional to continental scales, *J. Geophys. Res.*, 99(B7), 13,971–13,986, doi:10.1029/94JB00744.
- Hulme, M. (1992), A 1951–80 global land precipitation climatology for the evaluation of general circulation models, *Clim. Dyn.*, 7, 57–72, doi:10.1007/BF00209609.
- Kirchner, J. W., et al. (2001), Mountain erosion over 10 yr, 10 k.y., and 10 m.y. time scales, *Geology*, 29(7), 591–594, doi:10.1130/0091-7613(2001)029<0591:MEOYKY>2.0.CO;2.
- Kooi, H., and C. Beaumont (1996), Large-scale geomorphology: Classical concepts reconciled and integrated with contemporary ideas via a surface processes model, *J. Geophys. Res.*, 101(B2), 3361–3386, doi:10.1029/95JB01861.
- Lague, D., A. Crave, and P. Davy (2003), Laboratory experiments simulating the geomorphic response to tectonic uplift, *J. Geophys. Res.*, 108(B1), 2008, doi:10.1029/2002JB001785.
- Lague, D., N. Hovius, and P. Davy (2005), Discharge, discharge variability, and the bedrock channel profile, *J. Geophys. Res.*, 110, F04006, doi:10.1029/2004JF000259.
- Lavé, J. (2005), Analytic solution of the mean elevation of a watershed dominated by fluvial incision and hillslope landslides, *Geophys. Res. Lett.*, 32, L11403, doi:10.1029/2005GL022482.
- Ludwig, W., and J.-L. Probst (1998), River sediment discharge to the oceans: Present-day controls and global budgets, *Am. J. Sci.*, 298, 265–295.
- Meade, R. H., and R. S. Parker (1985), Sediments in rivers of the United States, *U.S. Geol. Surv. Water Supply Pap.*, 2275, 49–60.
- Métivier, F., and Y. Gaudemer (1999), Stability of output fluxes of large rivers in South and East Asia during the last 2 million years: Implications on floodplain processes, *Basin Res.*, 11(4), 293–303, doi:10.1046/j.1365-2117.1999.00101.x.
- Meunier, P., et al. (2006), Flow pattern and sediment transport in a braided river: The “torrent de St Pierre” (French Alps), *J. Hydrol.*, 330, 496–505, doi:10.1016/j.jhydrol.2006.04.009.
- Miller, K. G., et al. (2005), The Phanerozoic record of global sea-level change, *Science*, 310, 1293–1298, doi:10.1126/science.1116412.
- Milliman, J. D., and J. P. M. Syvitski (1992), Geomorphic / tectonic control of sediment discharge to the ocean: The importance of small mountain rivers, *J. Geol.*, 100, 525–544, doi:10.1086/629606.
- Millot, R., et al. (2002), The global control of silicate weathering rates and the coupling with physical erosion: New insights from rivers of the Canadian Shield, *Earth Planet. Sci. Lett.*, 196, 83–98, doi:10.1016/S0012-821X(01)00599-4.
- Ohmori, H. (2003), The paradox of equivalence of the Davisian end-peneplain and Penckian primary peneplain, in *Concepts and Modelling in Geomorphology: International Perspectives*, edited by I. S. Evans et al., pp. 3–32, Terrapub, Tokyo.
- Ouimet, W. B., et al. (2009), Beyond threshold hillslopes: Channel adjustment to base-level fall in tectonically active mountain ranges, *Geology*, 37, 579–582, doi:10.1130/G30013A.1.
- Padgett, G. V., and R. Ehrlich (1976), Paleohydrologic analysis of a late Carboniferous fluvial system, Southern Morocco, *Geol. Soc. Am. Bull.*, 87, 1101–1104, doi:10.1130/0016-7606(1976)87<1101:PAOALC>2.0.CO;2.
- Paola, C., and D. Mohrig (1996), Palaeohydraulics revisited: Palaeoslope estimation in coarse-grained braided rivers, *Basin Res.*, 8, 243–254, doi:10.1046/j.1365-2117.1996.00253.x.
- Pazzaglia, F. J., and M. T. Brandon (1996), Macrogeomorphic evolution of the post-Triassic Appalachian mountains determined by deconvolution of the offshore basin sedimentary record, *Basin Res.*, 8(3), 255–278, doi:10.1046/j.1365-2117.1996.00274.x.
- Pelletier, J. D. (2004), The influence of piedmont deposition on the time scale of mountain-belt denudation, *Geophys. Res. Lett.*, 31, L15502, doi:10.1029/2004GL020052.
- Pinet, P., and M. Souriau (1988), Continental erosion and large-scale relief, *Tectonics*, 7, 563–582, doi:10.1029/TC007i003p00563.
- Riebe, C. S., et al. (2001), Minimal climatic control on erosion rates in the Sierra Nevada, *Calif. Geol.*, 29(5), 447–450.
- Riebe, C. S., et al. (2004), Erosional and climatic effects on long-term chemical weathering rates in granitic landscapes spanning diverse climate regimes, *Earth Planet. Sci. Lett.*, 224, 547–562, doi:10.1016/j.epsl.2004.05.019.
- Rouby, D., et al. (2009), Sediment supply to the Orange sedimentary system over the last 150 My: An evaluation from sedimentation/denudation balance, *Mar. Pet. Geol.*, 26(6), 782–794, doi:10.1016/j.marpetgeo.2008.08.004.
- Rowley, D. B., and C. N. Garzione (2007), Stable-isotope paleoaltimetry, *Annu. Rev. Earth Planet. Sci.*, 35, 463–508, doi:10.1146/annurev.earth.35.031306.140155.
- Schaller, M., et al. (2001), Large-scale erosion rates from in situ-produced cosmogenic nuclides in European river sediments, *Earth Planet. Sci. Lett.*, 188, 441–458, doi:10.1016/S0012-821X(01)00320-X.
- Schumm, S. A. (1985), Patterns of alluvial rivers, *Annu. Rev. Earth Planet. Sci.*, 13, 5–27, doi:10.1146/annurev.earth.13.050185.000253.
- Schumm, S. A., and H. R. Khan (1972), Experimental study of channel patterns, *Geol. Soc. Am. Bull.*, 83, 1755–1770, doi:10.1130/0016-7606(1972)83[1755:ESOC]2.0.CO;2.
- Sepulchre, P., et al. (2006), Tectonic uplift and eastern Africa aridification, *Science*, 313, 1419–1423, doi:10.1126/science.1129158.
- Simoës, M., J. P. Avouac, O. Beyssac, B. Goffé, K. A. Farley, and Y.-G. Chen (2007), Mountain building in Taiwan: A thermokinematic model, *J. Geophys. Res.*, 112, B11405, doi:10.1029/2006JB004824.



- Sklar, L. S., and W. E. Dietrich (2004), A mechanistic model for river incision into bedrock by saltating bed load, *Water Resour. Res.*, **40**, W06301, doi:10.1029/2003WR002496.
- Sklar, L. S., and W. E. Dietrich (2006), The role of sediment in controlling steady-state bedrock channel slope: Implications of the saltation-abrasion incision model, *Geomorphology*, **82**, 58–83, doi:10.1016/j.geomorph.2005.08.019.
- Summerfield, M. (2007), Constraining the surface uplift and denudational record of southern Africa, in *TOPOAFRICA - Evolution of African topography over the last 250 My*, *Mem. Geosci. Rennes*, vol. X, edited by J. Braun et al., pp. xx–xx, Géosci. Rennes, UMR 6118, Univ. Rennes 1, Rennes, France.
- Summerfield, M. A., and N. J. Hulton (1994), Natural controls of fluvial denudation rates in major world drainage basins, *J. Geophys. Res.*, **99**(B7), 13,871–13,883, doi:10.1029/94JB00715.
- Syvitski, J. P. M., and J. D. Milliman (2007), Geology, geography, and humans battle for dominance over the delivery of fluvial sediment to the coastal ocean, *J. Geol.*, **115**, 1–19, doi:10.1086/509246.
- Tucker, G. E. (2004), Drainage basin sensitivity to tectonic and climatic forcing: Implications of a stochastic model for the role of entrainment and erosion threshold, *Earth Surf. Processes Landforms*, **29**, 185–205, doi:10.1002/esp.1020.
- Tucker, G. E., and R. L. Bras (1998), Hillslope processes, drainage density, and landscape morphology, *Water Resour. Res.*, **34**(10), 2751–2764, doi:10.1029/98WR01474.
- Tucker, G. E., and G. R. Hancock (2010), Modelling landscape evolution, *Earth Surf. Processes Landforms*, **35**, 28–50, doi:10.1002/esp.1952.
- Tucker, G. E., and R. L. Slingerland (1997), Drainage basin responses to climate change, *Water Resour. Res.*, **33**(8), 2031–2047, doi:10.1029/97WR00409.
- von Blanckenburg, F. (2005), The control mechanisms of erosion and weathering at basin scale from cosmogenic nuclides in river sediment, *Earth Planet. Sci. Lett.*, **237**, 462–479, doi:10.1016/j.epsl.2005.06.030.
- von Blanckenburg, F., T. Hewawasam, and P. W. Kubik (2004), Cosmogenic nuclide evidence for low weathering and denudation in the wet, tropical highlands of Sri Lanka, *J. Geophys. Res.*, **109**, F03008, doi:10.1029/2003JF000049.
- Whipple, K. X., and B. J. Meade (2004), Controls on the strength of coupling among climate, erosion, and deformation in two-sided, frictional orogenic wedges at steady state, *J. Geophys. Res.*, **109**, F01011, doi:10.1029/2003JF000019.
- Whipple, K. X., and B. J. Meade (2006), Orogen response to changes in climatic and tectonic forcing, *Earth Planet. Sci. Lett.*, **243**, 218–228, doi:10.1016/j.epsl.2005.12.022.
- Whipple, K. X., and G. E. Tucker (1999), Dynamics of the stream-power river incision model: Implications for height limits of mountain ranges, landscape response timescales, and research needs, *J. Geophys. Res.*, **104**(B8), 17,661–17,674, doi:10.1029/1999JB900120.
- Willett, S. D., and M. T. Brandon (2002), On steady states of mountain belts, *Geology*, **30**(2), 175–178, doi:10.1130/0091-7613(2002)030<0175:OSSIMB>2.0.CO;2.